Draft version May 18, 2016
Preprint typeset using LaTeX style AASTeX6 v. 1.0

UPDATED PHOTOMETRY FOR THE KINGFISH SAMPLE OF NEARBY GALAXIES

D. A. Dale[1], M. Boquien[8], D. Calzetti[10], D. O. Cook[1], M. Galametz[12], K. D. Gordon[13], J. L. Hinz[3], L. K. Hunt[15], R. C. Kennicutt[12], H. Roussel[5], J. A. Turner[1], C. D. Wilson[19], et al.

[1]Department of Physics & Astronomy, University of Wyoming, Laramie, USA; ddale@uwyo.edu

ABSTRACT

We present an update to the complete ultraviolet/optical/infrared/submillimeter/radio database of global photometry for the 79 nearby galaxies that comprise the union of the KINGFISH and SINGS samples. The dataset presented here includes contributions from *GALEX*, *SDSS*, *2MASS*, *WISE*, *Spitzer*, *Herschel*, *SCUBA*, and the *VLA*. Improvements of note include recalibrations of previously-published SINGS BVR_CI_C and KINGFISH far-infrared/submillimeter photometry.

Keywords: ISM: general — galaxies: ISM — infrared: ISM

1. INTRODUCTION

Access to panchromatic photometry for galaxies is crucial to fully understanding the characteristics of, and relative contributions to, galaxy broadband spectra from the various processes related to star formation and the accretion disks that feed supermassive black holes (Silva et al. 1998; da Cunha et al. 2008; Boquien 2016). Though a fairly complete multi-wavelength dataset has been published for the SINGS sample of 75 nearby galaxies (Kennicutt et al. 2003; Dale et al. 2005, 2007), subsequent far-infrared/submillimeter *Herschel* broadband data were later published for the KINGFISH sample of 61 nearby galaxies (Kennicutt et al. 2011; Dale et al. 2012), a sample for which 57 of the 61 targets are also SINGS targets. The photometric datasets from the combined SINGS/KINGFISH surveys have served as important references for studies seeking to understand the diverse properties of galaxies in the Local Universe (da Cunha et al. 2008; Noll et al. 2009; Jonsson et al. 2010; Rémy-Ruyer et al. 2015), or to serve as redshift-zero comparators to higher redshift galaxies (Kartaltepe et al. 2010; Maiolino et al. 2015; Scoville et al. 2016). However, the calibration of a portion of the SINGS BVR_CI_C from Dale et al. (2007) are suspect, and the calibration of the *Herschel* photometers have undergone multiple revisions since 2012.

In this effort we present an update to the global (spatially-integrated) photometry for the 79 nearby galaxies that comprise the union of the KINGFISH and SINGS samples. This update includes a Pan-STARRS1-based recalibration of previously-published BVR_CI_C fluxes. We also include new *ugriz* and 12 μm photometry, respectively, from the *Sloan Digital Sky Survey* (*SDSS*) and the *WISE* mission. In addition, the *Herschel* PACS photometry for KINGFISH galaxy NGC 0584 was not included in Dale et al. (2012) since those imaging data were not yet taken. Furthermore, we include new Herschel photometry for six SINGS galaxies from the Herschel Very Nearby Galaxy Survey (PI C. Wilson) that are not in the KINGFISH sample (NGC 2403, M81=NGC 3031, M82=NGC 3034, NGC 4125, M51a=NGC 5194, and M51b=NGC 5195). Finally, we complete the presentation of a multi-wavelength database by including previously published global photometry from ultraviolet (*GALEX*), infrared (*2MASS*, *Spitzer*), and radio (VLA) wavelengths.

Section 2 provides a brief overview of the galaxy sample, Section 3 recaps the relevant observations and approaches to data processing, Section 4 describes the salient results, and Section 5 provides the summary.

2. GALAXY SAMPLE

Table 5 presents the full list of 79 galaxies that form the union of the SINGS and KINGFISH samples. These galaxies were selected to span a range of morphologies, colors, and luminosities (e.g., Figures 5 and 3, respectively, of Kennicutt et al. 2003; Dale et al. 2012). The distances reach out to $\sim$ 30 Mpc with a median value of $\sim$ 10 Mpc. The sample was chosen to be a representative sampling of the Local Universe; the sample is not volume-limited and thus does not represent a statistical sampling of the Local Volume. The sample is comprised of 8%, 11%, 63%, and 18% early-type, lenticular, spiral, and irregular galaxies, respectively, based on the optical morphologies provided in the NASA/IPAC Extragalactic Database (NED). This galaxy sample has no sources for which the optical luminosity is dominated by AGN emission, though one-third have signatures of Seyfert/LINER nuclei (Dale et al. 2006; Moustakas et al. 2010). There are only a few galaxies that are obviously interacting with neighboring galaxies

including NGC 5194 (with NGC 5195), NGC 1316 (with NGC 1317), and NGC 3190 (with NGC 3187).

3. OBSERVATIONS AND DATA PROCESSING

Much of the photometry presented here has already been described in Dale et al. (2007) and Dale et al. (2012), so we focus the below discussion on important differences from what is presented in those publications.

3.1. *Optical*

Some of the optical $BVR_{\rm C}I_{\rm C}$ photometry from Dale et al. (2007) suffer from faulty calibration (Muñoz-Mateos et al. 2009). Sometimes not enough standard star observations were taken, sometimes the standards were saturated, and some of the frames taken in non-photometric conditions were not successfully calibrated *a posteriori*. A recalibration is carried out here via comparison of photometry on foreground stars in Pan-STARRS1 (PS1) $g_{\rm PS1}r_{\rm PS1}i_{\rm PS1}z_{\rm PS1}$ and in our 2007-era $BVR_{\rm C}I_{\rm C}$ imaging. Care was taken in the comparison to only use bright ($r_{\rm PS1}$<19 mag), unsaturated sources with PSFs that agree with the seeing profiles of each image (i.e., background galaxies are excluded). The median number of foreground stars per galaxy utilized for this purpose was 15. Aperture diameters for the foreground stellar photometry were typically 7″; increasing the aperture diameter by 50% results in a <1% difference in the calibration. The PS1 fluxes were converted from their measured values at 1.2 airmasses to 0 airmasses (Table 4 of Tonry et al. 2012), and the small (tens of millimag) corrections suggested by Scolnic et al. (2015) were incorporated (see their Table 3).

We adopted the Tonry et al. (2012) quadratic filter transformations for stars between Pan-STARRS1 $g_{\rm PS1}r_{\rm PS1}i_{\rm PS1}z_{\rm PS1}$ and $BVR_{\rm C}I_{\rm C}$, though very similar results are obtained when using linear transformations between *SDSS* and Johnson/Cousins filters (Jester et al. 2005; Lupton et al. 2005; Chonis & Gaskell 2008; Jordi et al. 2006; Tonry et al. 2012). The only significant outliers for any of these various transformations are the Chonis & Gaskell (2008) V and Lupton et al. (2005) $R_{\rm C}$ stellar transformations, both of which yield calibrations that ultimately result in galaxy fluxes that are 25–30% ($\sim 0.25-0.30$ mag) brighter compared to when using other published transformations. The photometric calibrations are derived in practice from the error-weighted differences between the instrumental $BVR_{\rm C}I_{\rm C}$ fluxes and the measured PS1 fluxes (transformed to $BVR_{\rm C}I_{\rm C}$) for the suite of suitable foreground stars identified for each galaxy. The dispersions in these bootstrap calibrations range from 2% to 15% (with a median of 5%) and contribute to the overall photomeric uncertainty estimates; the photometric uncertainties for the PS1-recalibrated fluxes are the sums in quadrature of these dispersions along with the uncertainties in the published $g_{\rm PS1}r_{\rm PS1}i_{\rm PS1}z_{\rm PS1}$ $\rightarrow$ $BVR_{\rm C}I_{\rm C}$ transformations and the instrumental galaxy flux measurements.

The Pan-STARRS1 survey does not encompass regions of the sky south of $\delta < -30°$, and thus PS1 calibration is not possible for 18 SINGS/KINGFISH objects. Table 3 indicates for which targets the $BVR_{\rm C}I_{\rm C}$ photometry has been re-calibrated via PS1. Additional optical photometry is of course possible via *SDSS*. *SDSS ugriz* imaging (Data Release 12) is used to provide optical fluxes for 51 of the 79 SINGS/KINGFISH galaxies. The union of the *SDSS ugriz* and PS1-recalibrated $BVR_{\rm C}I_{\rm C}$ samples comprises 63 galaxies, or 80% of the full sample. The fraction of the sample for which we have reliable optical photometry approaches 100% after inclusion of $BVR_{\rm C}I_{\rm C}$ photometry from other global photometric datasets (see Table 3 and de Vaucouleurs et al. 1991; Muñoz-Mateos et al. 2009; Tully et al. 2009; Cook et al. 2014).

Other differences between our $BVR_{\rm C}I_{\rm C}$ photometry and those appearing in Dale et al. (2007) include the use of SINGS Data Release 4 (DR4) images (DR2 imaging was used in the previous publication), more robust sky level determinations (i.e., a significantly larger number of sky pixels are now used), and a fresh take on the editing of foreground stars and background galaxies. In some instances the DR4 images are noticeably flatter than their DR2 counterparts (e.g., NGC 0628 $VR_{\rm C}I_{\rm C}$). Otherwise, the data processing procedures are essentially identical to those already described in Dale et al. (2007).

3.2. *Herschel Infrared*

Fluxes based on *Herschel* PACS and SPIRE imaging are presented here for 67 of the 79 SINGS/KINGFISH galaxies. The *Herschel* PACS and SPIRE imaging observations are described in Dale et al. (2012) for the 61 KINGFISH galaxies, except for the PACS observations of NGC 0584 which were taken too late to appear in that publication. Another minor difference from Dale et al. (2012) is that the PACS maps utilized here are deeper for five KINGFISH objects since we have now incorporated additional data from other observing programs: Holmberg II, IC 2574, NGC 2798, NGC 4236, and NGC 4631. This allows for some diffuse flux to be additionally detected, and for the faint Holmberg II it makes an appreciable relative difference in the global fluxes (see § 4). We also incorporate here new *Herschel* imaging observations for six SINGS galaxies from the Herschel Very Nearby Galaxy Survey (PI C. Wilson) that are

not in the KINGFISH sample: NGC 2403, M81=NGC 3031, M82=NGC 3034, NGC 4125, M51a=NGC 5194, and M51b=NGC 5195. The observing procedures for these six galaxies ... *input from C. Wilson here.*

The *Herschel* PACS and SPIRE imaging data for these $61+6=67$ galaxies for this publication were processed from Level 0 to Level 1 using HIPE Version 11.1.0, and the Level 1-to-Level 2 post-pipeline processing utilized Scanamorphos Version 24.0 (Roussel 2013). With this newer version of Scanamorphos, the PACS distortion flatfield is now properly incorporated. In practice, this has decreased the noise levels in the maps and changed the flux calibration by $\sim 1\%$, 1%, and 7% at 70, 100, and 160 μm, respectively. Moreover, the de-striping of PACS observations of large and diffuse fields is substantially improved, and the subtraction of the average drift on short timescales no longer introduces low-level noise. These changes allow for more secure detections of diffuse emission and more robust estimates of sky levels.

One important factor involved in the SPIRE flux calibration is the SPIRE beam size, since the SPIRE images are converted to surface brightness units by dividing by the estimated beam areas. The beam sizes used for Dale et al. (2012) were 423, 751, and 1587 $\square''$ compared to the updated values of 465.39, 822.58, 1768.66 $\square''$ for this work at 250, 350, and 500 μm, respectively. These are the recommended beam size values in Version 2.5 (24 March 2014) of the SPIRE Handbook.

The PACS calibration uncertainties are $\epsilon_{\mathrm{cal},\nu}/f_\nu \sim 5\%$, according to Version 2.5.1 (09 July 2013) of the PACS Observer's Manual. Calibration uncertainties for SPIRE data are estimated at $\epsilon_{\mathrm{cal}}/f_\nu \approx 7\%$, also taken from Version 2.5 of the SPIRE Observer's Manual. This level of uncertainty in the SPIRE calibration is a sum in quadrature of the uncertainties in the absolute and relative calibrations ($\sim$5.5%) along with the uncertainties in the extended source calibration ($\sim$4%).

3.3. *WISE 12 μm*

WISE 12 μm imaging (Wright et al. 2010) is utilized here to help bridge the gap in wavelength coverage in our broadband SEDs between the *Spitzer* 8 and 24 μm bandpasses. The 12 μm bandpass is an important tracer of the PAH complexes centered near (restframe) wavelengths of 11.3, 12.7, and 17 μm (Smith et al. 2007). At 12 μm, the *WISE* PSF FWHM is $6\farcs5$ and the photometric calibration $\sim$10% (Wright et al. 2010). Mention here the calibration and aperture correction factors? color correction, too?

3.4. *Ancillary Ultraviolet, Submillimeter, and Radio Data*

3.5. *Sky Estimation and Subtraction*

See my description in Dale2016 for an updated version of this old 2012 text.

The "sky" in the direction of any galaxy is a superposition of emission from foreground stars, interstellar emission, background galaxies, and in the case of ground-based observations, the Earth's atmosphere. To determine the sky level for each image, a set of sky apertures has been defined that collectively circumscribe the galaxy, projected on the sky close enough to the galaxy to measure the "local" sky but far enough away to avoid containing any galaxy emission (see Figure 1 Dale et al. 2012). The emission from any prominent neighboring and/or background galaxies that are projected to lie within the sky apertures is removed before the sky is estimated. The total sky area, derived from the sum of the areas from all sky apertures, is typically significantly greater than that covered by the galaxy aperture itself, thereby limiting the contribution of uncertainty in the sky level to the overall error budget. The mean sky level per pixel is computed from the collection of these sky apertures, the value is scaled to the number of pixels in the galaxy aperture, and the result is subtracted off from the overall galaxy aperture counts (all done within IRAF/`IMCNTS`).

Aniano et al. (2012) follow a different procedure for subtracting the sky emission from KINGFISH imaging, including fitting a tilted plane to the sky for each galaxy instead of a single value approach adopted here. Aniano et al. (2012) study the spatial variations in the far-infrared/sub-millimeter spectral energy distributions and thus a more detailed characterization of the local sky is necessary. The effects of most sky gradients cancel out in extracting spatially integrated fluxes; the two approaches yield generally consistent global fluxes.

3.6. *Aperture Photometry*

The elliptical apertures used for global photometry are listed in Table 5, and the same aperture is used to extract the flux at each wavelength. The apertures were chosen to encompass essentially all of the emission at every wavelength. The average ratio of aperture major axis length $2a$ to the de Vaucouleurs D_{25} optical major axis is 1.45 (with a 1σ dispersion in this ratio of 0.45).

Prior to extracting fluxes from aperture photometry, any emission from neighboring or background galaxies is identified and removed from the area covered by each aperture. The identification is assisted by ancillary data at

shorter wavelengths and higher spatial resolution (e.g., *Spitzer*/IRAC 3.6 and 8.0 μm, *HST* optical, and ground-based Hα imaging). The removal is accomplished via IRAF/`IMEDIT` by replacing the values of contaminated pixels with the values from a random selection of nearby sky pixels, thereby incorporating the same noise statistics as the sky. Usually the removal of such emission affects the global flux at less than the 1% level, but in a few cases the impact is quite important, e.g., NGC 1317 lies within the aperture of NGC 1316, and background galaxies in the fields of the fainter dwarfs like Ho II and DDO 053 would contribute significantly to the integrated flux (by up to $\sim 30-50\%$) if not removed (see also Walter et al. 2007).

At the longest wavelengths where the imaging resolution is typically coarsest, a small portion of the galaxy emission may appear beyond the chosen apertures. Thus, for the *Spitzer* MIPS and *Herschel* photometry we develop aperture corrections to mitigate this effect. Aperture corrections are empirically determined from a comparison of fluxes from smoothed and unsmoothed *Spitzer*/IRAC 3.6 μm imaging, which has a native resolution of $\sim$1.″5. The aperture correction at a given MIPS, PACS, or SPIRE wavelength is the ratio of the flux from the unsmoothed 3.6 μm image to the flux from the 3.6 μm image smoothed to the PSF at the wavelength in question. The amplitudes of the global photometry aperture corrections are typically quite small, with median values of 1.0 and maximum values of 1.03 for PACS and between 1.07 and 1.13 for SPIRE. This technique assumes that a galaxy's profile in the far-infrared matches that of its (mostly) stellar profile in the near-infrared, and there may in fact be appreciable differences in the two emission profiles. What about the ap corr values for Spitzer? And didn't I use 8um for ap corrs somewhere? Might be better to use dust instead of stars for ap corrs! DId I do ap corrs for optical data in D07?

The uncertainties in the integrated photometry $\epsilon_{\rm total}$ are computed as a combination in quadrature of the calibration uncertainty $\epsilon_{\rm cal}$ and the measurement uncertainty $\epsilon_{\rm sky}$ based on the measured sky fluctuations and the areas covered by the galaxy and the sum of the sky apertures, i.e.,

$$\epsilon_{\rm total} = \sqrt{\epsilon_{\rm cal}^2 + \epsilon_{\rm sky}^2} \tag{1}$$

with

$$\epsilon_{\rm sky} \ = \sigma_{\rm sky}\Omega_{\rm pix}\ \sqrt{N_{\rm pix} + {N_{\rm pix}}^2/N_{\rm sky}} \tag{2}$$

where $\sigma_{\rm sky}$ is the standard deviation of the sky surface brightness fluctuations, $\Omega_{\rm pix}$ is the solid angle subtended per pixel, and $N_{\rm pix}$ and $N_{\rm sky}$ are the number of pixels in the galaxy and (the sum of) the sky apertures, respectively. For the few sources undetected by *Herschel* imaging, 5σ upper limits are derived assuming a galaxy spans all $N_{\rm pix}$ pixels in the aperture,

$$f_\nu(5\sigma \text{ upper limit}) \ = \ 5\ \epsilon_{\rm sky}. \tag{3}$$

Why didn't I also incorporate sky uncertainties from region-to-region fluctuations? Was it producing unrealistically large values, or were they too small b/c I was using a different eqn that ignored N_{ap}?

4. RESULTS

4.1. *Flux Densities*

Table 2a presents the spatially-integrated flux densities for all 79 SINGS+KINGFISH galaxies for 30 photometric bands. The tabulated flux densities include aperture corrections (§ 3.6) and are *not* corrected for Galactic extinction. No color corrections have been applied to the data in Table 2a. Some of the fluxes presented here remain unchanged from the values published elsewhere, for example *2MASS JHK*$_{\rm s}$ *Spitzer* IRAC and MIPS, *SCUBA* 850 μm, and VLA 20 cm photometry. However, if any differences exist between values published in multiple publications, precedence is given to the more recent published values, e.g., *2MASS* and *Spitzer* photometry from the Local Volume Legacy publication of Dale et al. (2009) is given priority over the photometry appearing in Dale et al. (2007).

Figures 1 and 2 provide comparisons of our updated optical and infrared fluxes with those presented in previous publications. The updated SPIRE beam sizes are larger than those used in Dale et al. (2012) by [10.0,9.5,11.4]% at [250,350,500] μm, which naturally leads to smaller SPIRE fluxes. This decrease is evident in Figure 2, where the average SPIRE flux is $\sim$[6,4,14]% at [250,350,500] μmthan what appeared in Dale et al. (2012). For the five galaxies where we incorporated additional PACS data from other observing programs (Holmberg II, IC 2574, NGC 2798, NGC 4236, and NGC 4631; see § 3), the resulting PACS maps are deeper and thus allow for some diffuse flux to be additionally detected. For faint Holmberg II it makes an appreciable relative difference: the 70 and 100 μm global fluxes are now 40-50% larger.

4.2. *The Observed Spectral Energy Distributions*

Figure 3 shows the observed infrared/sub-millimeter spectral energy distributions for the KINGFISH sample. Included in each panel, when available, are the *GALEX* far- and near-ultraviolet, $BVR_{\rm C}I_{\rm C}$ and *ugriz* optical, *2MASS* $JHK_{\rm s}$ near-infrared, *Spitzer* 3.6, 4.5, 5.8, 8.0, 24, 70, and 160 μm, *Herschel* 70, 100, 160, 250, 350, and 500 μm, and *SCUBA* 850 μm fluxes.

4.3. *Fits to the Observed Spectral Energy Distributions*

To extract physical parameters from the broadband spectral data, the spectral energy distributions were fitted with the models of Draine & Li (2007), models based on mixtures of amorphous silicate and graphitic dust grains that effectively reproduce the average Milky Way extinction curve and are consistent with observations of PAH features and the variety of infrared continua in local galaxies.

4.4. *Spectral Energy Distribution Fit Parameters*

4.5. *Sub-millimeter Excess*

Is the excess still there?

$$\xi(500\mu{\rm m}) = \frac{\nu f_\nu(500\mu{\rm m})_{\rm observed} - \nu f_\nu(500\mu{\rm m})_{\rm model}}{\nu f_\nu(500\mu{\rm m})_{\rm model}}. \quad (4)$$

Only three galaxies show an excess above 0.60 whereas previously it was a dozen galaxies when the prior photometry and calibrations were utilized in the SED fits. This is consistent with kirkpatrick13.

5. DISCUSSION AND SUMMARY

An update to the full panchromatic photometric database is presented. Drawing on the SINGS heritage of KINGFISH, spatially-integrated fluxes from the ultraviolet through the radio are provided.

How do the fluxes compare to those previously published?

Is there still a submm excess like I claimed or did it mostly go away like Kirkpatrick suggests?

Herschel is an ESA space observatory with science instruments provided by European-led Principal Investigator consortia and with important participation from NASA. This work is based on observations made with the *Spitzer Space Telescope* and utilizes the NASA/IPAC Infrared Science Archive, both operated by JPL/Caltech under a contract with NASA. We gratefully acknowledge NASA's support for construction, operation, and science analysis for the GALEX mission, developed in cooperation with the Centre National d'Etudes Spatiales of France and the Korean Ministry of Science and Technology. Funding for the Sloan Digital Sky Survey and SDSS-II has been provided by the Alfred P. Sloan Foundation, the Participating Institutions, the NSF, the U.S. Department of Energy, NASA, the Japanese Monbukagakusho, the Max Planck Society, and the Higher Education Funding Council for England. This publication makes use of data products from the Wide-field Infrared Survey Explorer, which is a joint project of the University of California, Los Angeles, and the JPL/Caltech, funded by NASA. The Pan-STARRS1 Surveys have been made possible through contributions of the Institute for Astronomy, the University of Hawaii, the Pan-STARRS Project Office, the Max-Planck Society and its participating institutes, the Max Planck Institute for Astronomy, Heidelberg and the Max Planck Institute for Extraterrestrial Physics, Garching, The Johns Hopkins University, Durham University, the University of Edinburgh, Queen's University Belfast, the Harvard-Smithsonian Center for Astrophysics, the Las Cumbres Observatory Global Telescope Network Incorporated, the National Central University of Taiwan, the Space Telescope Science Institute, the NSF, the University of Maryland, and Eotvos Lorand University and the Los Alamos National Laboratory.

REFERENCES

Aniano, G., et al. 2012, ApJ, 756, 138
Boquien, M. 2016, MNRAS, in prep
Chonis, T. S., & Gaskell, C. M. 2008, AJ, 135, 264
Cook, D. O., et al. 2014, MNRAS, 445, 881
da Cunha, E., Charlot, S., & Elbaz, D. 2008, MNRAS, 388, 1595
Dale, D. A., Helou, G., Magdis, G. E., Armus, L., D´ıaz-Santos, T., & Shi, Y. 2014, ApJ, 784, 83
Dale, D. A., et al. 2005, ApJ, 633, 857
—. 2006, ApJ, 646, 161
—. 2007, ApJ, 655, 863
—. 2009, ApJ, 703, 517
—. 2012, ApJ, 745, 95
de Vaucouleurs, G., de Vaucouleurs, A., Corwin, Jr., H. G., Buta, R. J., Paturel, G., & Fouqué, P. 1991, Third Reference Catalogue of Bright Galaxies.
Draine, B. T., & Li, A. 2007, ApJ, 657, 810
Jester, S., et al. 2005, AJ, 130, 873
Jonsson, P., Groves, B. A., & Cox, T. J. 2010, MNRAS, 403, 17
Jordi, K., Grebel, E. K., & Ammon, K. 2006, A&A, 460, 339
Kartaltepe, J. S., et al. 2010, ApJ, 709, 572
Kennicutt, R. C., et al. 2011, PASP, 123, 1347
Kennicutt, Jr., R. C., et al. 2003, PASP, 115, 928

Lupton, R. H., et al. 2005, in Bulletin of the American Astronomical Society, Vol. 37, American Astronomical Society Meeting Abstracts, 1384
Maiolino, R., et al. 2015, MNRAS, 452, 54
Moustakas, J., Kennicutt, Jr., R. C., Tremonti, C. A., Dale, D. A., Smith, J.-D. T., & Calzetti, D. 2010, ApJS, 190, 233
Muñoz-Mateos, J. C., et al. 2009, ApJ, 703, 1569
Noll, S., Burgarella, D., Giovannoli, E., Buat, V., Marcillac, D., & Muñoz-Mateos, J. C. 2009, A&A, 507, 1793
Rémy-Ruyer, A., et al. 2015, A&A, 582, A121
Roussel, H. 2013, PASP, 125, 1126
Scolnic, D., et al. 2015, ApJ, 815, 117
Scoville, N., et al. 2016, ApJ, 820, 83
Silva, L., Granato, G. L., Bressan, A., & Danese, L. 1998, ApJ, 509, 103
Smith, J. D. T., et al. 2007, ApJ, 656, 770
Tonry, J. L., et al. 2012, ApJ, 750, 99
Tully, R. B., Rizzi, L., Shaya, E. J., Courtois, H. M., Makarov, D. I., & Jacobs, B. A. 2009, AJ, 138, 323
Walter, F., et al. 2007, ApJ, 661, 102
Wright, E. L., et al. 2010, AJ, 140, 1868

Table 1. Galaxy Sample

Galaxy	Alternative Name	Optical Morph.	$E(B-V)$ (mag.)	α_0 & δ_0 (J2000)	$2a$ ($''$)	$2b$ ($''$)	PA ($^\circ$)	D_{25} (Mpc)	TIR ($L_\odot$)
NGC0024	UGCA002	SAc	0.017	000955.9−245755	301	216	45	8.20	8.8
NGC0337	NGC0337	SBd	0.096	005950.7−073444	253	194	140	19.30	10.1
NGC0584	NGC0584	E4	0.036	013120.6−065205	326	278	60	20.80	8.8
NGC0628	M074	SAc	0.060	013642.4+154711	879	808	90	7.20	9.9
NGC0855	UGC01718	E	0.061	021403.7+275237	259	169	60	9.73	8.6
NGC0925	UGC01913	SABd	0.065	022713.6+333504	735	486	105	9.12	9.7
NGC1097	UGCA041	SBb	0.023	024618.0−301642	758	612	130	14.20	10.6
NGC1266	NGC1266	SB0	0.085	031600.6−022541	234	232	0	30.60	10.4
NGC1291	NGC1291	SB0/a	0.011	031717.9−410616	884	836	90	10.40	9.5
NGC1316	FornaxA	SAB0	0.018	032241.2−371210	864	583	50	21.00	9.9
NGC1377	NGC1377	S0	0.024	033639.0−205408	181	162	90	24.60	10.1
NGC1404	NGC1404	E1	0.010	033852.3−353540	524	369	149	20.20	···
IC0342	UGC02847	SABcd	0.480	034659.5+680539	1667	1439	100	3.28	10.1
NGC1482	NGC1482	SA0	0.034	035439.0−203009	349	310	119	22.60	10.6
NGC1512	NGC1512	SBab	0.009	040355.6−432149	1001	928	83	11.60	9.5
NGC1566		SABbc	0.008	042000.4−545615	552	435	40	18.00	10.6
NGC1705		SA0	0.007	045413.5−532137	167	120	40	5.80	8.0
NGC2146	UGC03429	Sbab	0.082	061835.6+782129	236	235	120	17.20	11.1
NGC2403	UGC03918	SABcd	0.034	073655.1+653534	1512	929	124	3.50	9.6
HolmbergII	UGC04305	Im	0.027	081910.8+704320	554	465	60	3.05	7.8
M081DwarfA		I?	0.018	082356.0+710145	78	78	90	3.50	···
DDO053	UGC04459	Im	0.033	083407.4+661043	155	142	90	3.61	7.0
NGC2798	UGC04905	SBa	0.017	091723.1+415957	235	232	90	25.80	10.6
NGC2841	UGC04966	SAb	0.013	092203.3+505837	629	334	150	14.10	10.1
NGC2915		I0	0.236	092609.4−763736	183	132	110	3.78	7.6
HolmbergI	UGC05139	IABm	0.044	094033.6+711120	264	219	63	3.90	7.1
NGC2976	UGC05221	SAc	0.062	094715.3+675509	541	353	144	3.55	8.9
NGC3049	UGC05325	SBab	0.033	095449.6+091614	218	160	29	19.20	9.5
NGC3031	M081	SAab	0.069	095531.8+690403	1628	1122	154	3.50	9.6
NGC3034	M082	I0	0.134	095552.1+694057	698	581	65	3.50	10.7
HolmbergIX	UGC05336	Im	0.068	095729.2+690250	247	180	40	3.50	···
NGC3077	UGC05398	I0pec	0.058	100317.5+684354	488	436	64	3.83	8.9
M081DwarfB	UGC05423	Im	0.068	100531.2+702151	134	90	139	3.60	6.5
NGC3190	UGC05559	SAap	0.022	101805.7+214957	334	196	117	19.30	9.8
NGC3184	UGC05557	SABcd	0.014	101815.6+412542	614	538	169	11.70	10.0
NGC3198	UGC05572	SBc	0.011	101954.8+453301	518	315	35	14.10	10.0
IC2574	UGC05666	SABm	0.031	102823.9+682505	864	486	59	3.79	8.3
NGC3265	UGC05705	E	0.021	103106.8+284751	184	175	50	19.60	9.4
Mrk33	UGC05720	Im	0.010	103231.2+542359	181	177	90	21.70	9.8

Table 1 continued on next page

Table 1 *(continued)*

Galaxy	Alternative Name	Optical Morph.	$E(B-V)$ (mag.)	α_0 & δ_0 (J2000)	$2a$ ($''$)	$2b$ ($''$)	PA ($^\circ$)	D_{25} (Mpc)	TIR ($L_\odot$)
NGC3351	M095	SBb	0.024	104358.1+114210	592	441	11	9.33	9.9
NGC3521	UGC06150	SABbc	0.049	110548.1−000127	926	455	165	11.20	10.5
NGC3621	UGCA232	SAd	0.069	111818.3−324855	791	555	160	6.55	9.9
NGC3627	M066	SABb	0.029	112013.4+125927	745	486	167	9.38	10.4
NGC3773	UGC06605	SA0	0.023	113813.1+120644	118	116	0	12.40	8.8
NGC3938	UGC06856	SAc	0.018	115250.3+440715	504	468	0	17.90	10.3
NGC4125	UGC07118	E6p	0.016	120805.8+651024	228	151	90	21.40	9.1
NGC4236	UGC07306	SBdm	0.013	121643.2+692719	1240	369	162	4.45	8.7
NGC4254	M099	SAc	0.033	121849.7+142519	519	420	60	14.40	10.6
NGC4321	M100	SABbc	0.023	122254.8+154907	558	483	40	14.30	10.5
NGC4450	UGC07594	SAab	0.024	122830.1+170454	401	284	180	20.00	9.9
NGC4536	UGC07732	SABbc	0.016	123427.5+021113	454	376	120	14.50	10.3
NGC4552	M089	E	0.035	123539.8+123323	306	306	90	4.90	7.7
NGC4559	UGC07766	SABcd	0.015	123558.1+275752	576	327	140	6.98	9.5
NGC4569	M090	SABab	0.040	123650.2+131001	593	327	21	9.86	9.7
NGC4579	M058	SABb	0.035	123743.8+114858	325	271	90	16.40	10.1
NGC4594	M104	SAa	0.044	123959.6−113726	767	669	90	9.08	9.6
NGC4625	UGC07861	SABmp	0.016	124154.8+411623	298	214	100	9.30	8.8
NGC4631	UGC07865	SBd	0.015	124204.2+323219	901	240	85	7.62	10.4
NGC4725	UGC07989	SABab	0.010	125027.7+252948	689	523	30	11.90	9.9
NGC4736	M094	SAab	0.015	125055.2+410652	944	899	0	4.66	9.8
DDO154	UGC08024	IBm	0.008	125407.6+270916	216	126	50	4.30	···
NGC4826	M064	SAab	0.036	125643.3+214048	716	427	114	5.27	9.6
DDO165	UGC08201	Im	0.021	130625.9+674229	263	161	90	4.57	···
NGC5033	UGC08307	SAc	0.010	131328.2+363534	729	467	180	13.30	10.3
NGC5055	M063	SAbc	0.015	131549.2+420147	1097	711	80	7.94	10.3
NGC5194	M051a	SABbc	0.030	132950.6+471307	1699	1129	15	8.20	10.6
NGC5195	M051b	SB0p	0.031	132959.4+471556	202	191	0	8.20	9.3
NGC5398	Tololo89	SBdm	0.056	140121.2−330402	198	146	0	7.66	8.6
NGC5457	M101	SABcd	0.007	140325.0+542429	1800	1446	37	6.70	10.3
NGC5408		IBm	0.059	140321.1−412241	256	209	67	4.80	8.3
NGC5474	UGC09013	SAcd	0.009	140500.8+533920	412	373	90	6.80	8.7
NGC5713	UGC09451	SABbcp	0.034	144011.4−001726	225	225	90	21.37	10.5
NGC5866	UGC09723	S0	0.012	150628.8+554551	500	306	129	15.30	9.7
IC4710		SBm	0.076	182838.9−665903	313	219	120	8.50	8.6
NGC6822	DDO229	IBm	0.199	194453.2−144811	1453	1100	150	0.60	7.8
NGC6946	UGC11597	SABcd	0.294	203449.2+600959	953	928	0	6.80	10.5
NGC7331	UGC12113	SAb	0.078	223704.3+342435	683	335	168	14.50	10.7
NGC7552	IC5294	SAc	0.012	231610.8−423505	441	325	120	22.30	11.0
NGC7793		SAd	0.017	235749.9−323525	716	526	98	3.91	9.3

NOTE—$2a$ and $2b$ are the lengths of the major and minor axes used in the elliptical aperture photometry described herein; the position angle of the aperture's major axis is measured east of north. The total infrared luminosity listed in the last column is derived from Equation 5 of Dale et al. (2014) and the 8, 24, 70, and 160 μm fluxes in 2a and assumes the distances provided in this table.

a

Table 2a. Global Flux Densities in Janskys Corrected for Neither Galactic Nor Intrinsic Extinction

Galaxy	FUV	NUV	B	V	R_C	I_C	u	g	r	i
$\lambda(\mu m)$	0.1528	0.2271	0.440	0.553	0.640	0.790	0.3557	0.4825	0.6261	0.7672
A_λ/A_V	2.586	2.994	1.3103	1.0	0.7884	0.5766	1.6415	1.2190	0.8487	0.6405
NGC0024	874±137E−3	113±017E−2	870±022E−2	113±002E−1	143±007E−1	188±008E−1	...	...	...	...
NGC0337	943±130E−3	186±025E−2	112±006E−1	119±005E−1	134±007E−1	162±018E−1	389±009E−2	928±019E−2	126±002E−1	144±003E−1
NGC0584	360±051E−4	200±027E−3	149±017E−1	293±023E−1	376±042E−1	551±051E−1	347±008E−2	163±003E−1	323±006E−1	462±009E−1
NGC0628	733±115E−2	990±152E−2	661±041E−1	141±006E+0	140±006E+0	216±012E+0	238±004E−1	608±012E−1	930±018E−1	120±002E+0
NGC0855	144±022E−3	301±046E−3	256±025E−2	399±039E−2	524±014E−2	...	110±003E−2	331±007E−2	542±011E−2	709±015E−2
NGC0925	475±065E−2	624±086E−2	339±017E−1	549±149E−1	538±045E−1	669±055E−1	...	...	...	...
NGC1097	353±050E−2	509±071E−2	406±014E−1	684±025E−1	945±034E−1	129±004E+0	...	...	...	...
NGC1266	045±006E−4	291±041E−4	200±013E−2	368±019E−2	488±037E−2	733±054E−2	...	...	...	...
NGC1291	757±118E−3	166±025E−2	604±022E−1	122±004E+0	176±006E+0	245±009E+0	...	...	...	...
NGC1316	307±042E−3	165±022E−2	837±030E−1	164±006E+0	235±008E+0	299±011E+0	...	...	...	...
NGC1377	...	...	230±012E−2	375±015E−2	478±033E−2	761±023E−2	...	...	...	...
NGC1404	956±132E−4	276±038E−3	178±006E−1	365±013E−1	525±019E−1	776±028E−1	...	...	...	...
IC0342	...	...	588±080E+0	...	...	...	...	...	...	...
NGC1482	391±061E−4	143±020E−3	567±031E−2	763±049E−2	105±010E−1	159±013E−1	...	...	...	...
NGC1512	169±026E−2	179±030E−2	151±005E−1	259±009E−1	359±013E−1	496±018E−1	...	...	...	...
NGC1566	540±075E−2	654±090E−2	359±013E−1	607±022E−1	709±026E−1	875±032E−1	...	...	...	...
NGC1705	166±026E−2	157±024E−2	274±010E−2	373±013E−2	406±014E−2	543±020E−2	...	...	...	...
NGC2146	...	...	163±020E−1	266±034E−1	...	615±017E−1	...	...	...	...
NGC2403	238±038E−1	296±045E−1	147±014E+0	227±032E+0	245±009E+0	318±008E+0	734±025E−1	170±005E+0	240±008E+0	296±010E+0
HoII	416±065E−2	467±071E−2	140±010E−1	161±007E−1	214±024E−1	316±051E−1	...	...	...	...
M81dwA	476±065E−4	567±078E−4	107±043E−3	950±420E−4	114±042E−3	144±062E−3	...	...	...	...
DDO053	273±042E−3	273±042E−3	746±181E−3	900±220E−3	592±194E−3	844±274E−3	296±017E−3	578±020E−3	649±022E−3	669±024E−3
NGC2798	109±015E−3	233±032E−3	317±028E−2	572±034E−2	670±034E−2	113±010E−1	907±030E−3	330±007E−2	623±013E−2	853±018E−2
NGC2841	128±017E−2	206±028E−2	458±021E−1	794±028E−1	104±007E+0	180±010E+0	118±002E−1	480±009E−1	972±019E−1	143±002E+0
NGC2915	124±017E−2	163±022E−2	517±051E−2	605±022E−2	865±031E−2	737±073E−2	...	...	...	...
HoI	510±080E−3	583±088E−3	136±034E−2	173±043E−2	162±047E−2	226±056E−2	...	...	...	...
NGC2976	198±031E−2	295±045E−2	278±018E−1	426±013E−1	533±034E−1	748±050E−1	100±002E−1	279±005E−1	465±009E−1	603±012E−1
NGC3049	...	449±062E−3	278±022E−2	394±019E−2	427±030E−2	561±053E−2	108±003E−2	263±006E−2	423±009E−2	531±011E−2
NGC3031	167±026E−1	239±036E−1	384±038E+0	742±074E+0	...	158±004E+1	128±004E+0	483±016E+0	930±031E+0	135±004E+1
NGC3034	274±043E−2	909±138E−2	183±030E+0	241±024E+0	330±044E+0	470±056E+0	639±021E−1	168±005E+0	323±011E+0	439±014E+0
HoIX	372±051E−3	499±069E−3	734±116E−3	667±133E−3	687±140E−3	100±033E−2	508±027E−3	100±003E−2	107±003E−2	125±004E−2
NGC3077	...	...	227±006E−1	...	614±016E−1	...	913±020E−2	323±006E−1	571±011E−1	764±015E−1
M81dwB	778±122E−4	105±016E−3	620±207E−3	790±255E−3	933±315E−3	929±257E−3	249±017E−3	572±020E−3	817±026E−3	962±029E−3
NGC3190	392±054E−4	180±024E−3	108±004E−1	192±005E−1	266±008E−1	415±016E−1	240±006E−2	110±002E−1	222±004E−1	330±006E−1
NGC3184	415±057E−2	556±077E−2	354±030E−1	498±021E−1	584±040E−1	757±042E−1	114±002E−1	333±006E−1	527±010E−1	685±013E−1
NGC3198	233±032E−2	284±039E−2	208±008E−1	259±013E−1	303±024E−1	405±033E−1	662±014E−2	178±003E−1	278±005E−1	357±007E−1
IC2574	491±077E−2	529±080E−2	157±021E−1	201±027E−1	195±031E−1	278±037E−1	...	...	...	...
NGC3265	552±076E−4	963±133E−4	121±015E−2	180±008E−2	228±021E−2	364±052E−2	399±019E−3	122±003E−2	219±005E−2	300±007E−2
Mrk33	407±056E−3	518±071E−3	203±014E−2	291±056E−2	343±074E−2	398±079E−2	...	...	...	...
NGC3351	175±027E−2	296±045E−2	330±041E−1	570±041E−1	738±053E−1	112±006E+0	980±021E−2	356±007E−1	657±013E−1	917±018E−1
NGC3521	208±033E−2	452±069E−2	756±029E−1	124±002E+0	164±002E+0	244±007E+0	214±004E−1	788±015E−1	145±002E+0	198±003E+0
NGC3621	714±104E−2	110±015E−1	555±020E−1	795±029E−1	912±033E−1	116±004E+0	...	...	...	...
NGC3627	304±047E−2	578±088E−2	826±047E−1	125±002E+0	150±013E+0	226±012E+0	245±005E−1	840±016E−1	146±002E+0	201±004E+0
NGC3773	410±056E−3	554±076E−3	181±009E−2	241±008E−2	272±022E−2	339±027E−2	848±027E−3	177±004E−2	268±006E−2	321±007E−2
NGC3938	...	363±050E−2	234±009E−1	324±006E−1	361±020E−1	501±017E−1	786±017E−2	217±004E−1	328±006E−1	421±008E−1
NGC4125	...	343±047E−3	215±003E−1	387±007E−1	523±012E−1	784±050E−1	...	...	...	...
NGC4236	685±107E−2	828±126E−2	359±031E−1	409±032E−1	493±039E−1	572±055E−1	...	...	...	...
NGC4254	...	618±085E−2	390±024E−1	535±016E−1	662±024E−1	808±027E−1	149±003E−1	381±007E−1	588±011E−1	741±014E−1
NGC4321	...	539±074E−2	481±022E−1	715±019E−1	936±044E−1	137±008E+0	169±003E−1	477±009E−1	797±016E−1	107±002E+0
NGC4450	...	538±074E−3	220±011E−1	394±011E−1	533±018E−1	799±033E−1	...	...	...	...
NGC4536	166±023E−2	219±030E−2	196±013E−1	285±024E−1	355±036E−1	534±103E−1	610±013E−2	181±003E−1	304±006E−1	405±008E−1
NGC4552	181±025E−3	464±064E−3	262±011E−1	470±011E−1	653±017E−1	998±054E−1	...	...	...	...
NGC4559	529±073E−2	646±089E−2	323±021E−1	414±012E−1	467±034E−1	584±041E−1	117±002E−1	292±005E−1	417±008E−1	516±010E−1
NGC4569	575±079E−3	196±027E−2	389±038E−1	623±062E−1	...	...	110±002E−1	415±008E−1	687±013E−1	969±019E−1
NGC4579	563±077E−3	120±016E−2	334±013E−1	591±023E−1	751±047E−1	111±006E+0	780±016E−2	338±006E−1	655±013E−1	941±018E−1
NGC4594	520±081E−3	162±025E−2	122±007E+0	274±036E+0	323±010E+0	487±030E+0	298±006E−1	144±002E+0	295±005E+0	435±008E+0
NGC4625	617±098E−3	799±123E−3	386±029E−2	551±049E−2	639±089E−2	826±059E−2	135±004E−2	360±008E−2	555±012E−2	707±015E−2
NGC4631	107±016E−1	133±020E−1	650±051E−1	847±032E−1	976±049E−1	122±005E+0	268±005E−1	609±012E−1	886±017E−1	111±002E+0
NGC4725	218±030E−2	296±041E−2	484±025E−1	850±022E−1	107±003E+0	166±007E+0	129±002E−1	496±010E−1	932±018E−1	134±002E+0
NGC4736	699±109E−2	922±140E−2	149±009E+0	225±006E+0	302±010E+0	442±024E+0	442±008E−1	170±003E+0	311±006E+0	433±008E+0

Table 2a continued on next page

Table 2a *(continued)*

Galaxy	FUV	NUV	B	V	R_C	I_C	u	g	r	i
$\lambda(\mu m)$	0.1528	0.2271	0.440	0.553	0.640	0.790	0.3557	0.4825	0.6261	0.7672
A_λ/A_V	2.586	2.994	1.3103	1.0	0.7884	0.5766	1.6415	1.2190	0.8487	0.6405
DDO154	438±068E−3	430±066E−3	108±029E−2	115±035E−2	123±030E−2	128±032E−2	473±020E−3	908±026E−3	103±003E−2	103±003E−2
NGC4826	130±020E−2	350±053E−2	109±009E+0	165±009E+0	206±019E+0	321±018E+0	269±005E−1	109±002E+0	201±004E+0	286±005E+0
DDO165	562±088E−3	787±120E−3	307±076E−2	293±029E−2	266±057E−2	350±129E−2	101±003E−2	236±005E−2	269±006E−2	296±007E−2
NGC5033	195±027E−2	256±035E−2	250±012E−1	403±022E−1	...	646±042E−1	...	...	...	...
NGC5055	413±064E−2	666±103E−2	850±085E−1	138±013E+0	188±005E+0	281±007E+0	302±006E−1	984±019E−1	177±003E+0	252±005E+0
NGC5194	134±021E−1	214±032E−1	149±017E+0	199±013E+0	230±022E+0	340±030E+0	551±018E−1	136±004E+0	218±007E+0	280±009E+0
NGC5195	195±031E−3	546±085E−3	419±048E−1	668±045E−1	863±082E−1	157±014E+0	136±004E−1	396±013E−1	773±026E−1	109±003E+0
NGC5398	712±098E−3	113±015E−2	594±059E−2	594±059E−2	457±045E−2	570±057E−2	...	...	...	...
NGC5457	369±***E−4	432±***E−4	207±017E+0	266±025E+0	290±008E+0	436±012E+0	781±015E−1	194±003E+0	280±005E+0	356±007E+0
NGC5408	...	...	700±070E−2	950±095E−2	...	...	...	...	...	...
NGC5474	247±038E−2	271±041E−2	128±007E−1	169±006E−1	183±012E−1	218±019E−1	511±011E−2	120±002E−1	170±003E−1	202±004E−1
NGC5713	497±068E−3	100±013E−2	104±007E−1	147±006E−1	188±006E−1	251±026E−1	335±007E−2	993±020E−2	164±003E−1	209±004E−1
NGC5866	636±088E−4	414±057E−3	245±011E−1	443±016E−1	556±038E−1	865±050E−1	583±012E−2	265±005E−1	506±010E−1	746±015E−1
IC4710	207±028E−2	301±041E−2	753±075E−2	991±099E−2	835±083E−2	...	...	...	...	...
NGC6822	249±034E−1	405±056E−1	138±007E+0	882±045E−1	190±006E+0	213±017E+0	...	...	...	...
NGC6946	161±022E−1	415±057E−1	183±018E+0	296±013E+0	...	567±055E+0	...	...	...	...
NGC7331	143±019E−2	296±041E−2	607±034E−1	894±017E−1	121±003E+0	191±008E+0	130±002E−1	507±010E−1	984±019E−1	143±002E+0
NGC7552	763±105E−3	151±021E−2	133±004E−1	224±008E−1	232±023E−1	218±021E−1	...	...	...	...
NGC7793	126±019E−1	149±022E−1	586±058E−1	803±080E−1	774±077E−1	680±068E−1	...	...	...	...

NOTE—The compact table entry format TUV±WXYEZ implies (T.UV±W.XY)×10^Z in Jy. Corrections for neither Galactic nor intrinsic extinction has been applied (see § 3). The uncertainties include both statistical and systematic effects. 5σ upper limits are provided for non-detections. No color corrections have been applied.

b

Table 2b. Global Flux Densities in Janskys Corrected for Neither Galactic Nor Intrinsic Extinction

Galaxy	z	J	H	K_S	IRAC	IRAC	IRAC	IRAC	WISE	MIPS
$\lambda(\mu m)$	0.9097	1.25	1.65	2.17	3.6	4.5	5.8	8.0	12	24
A_λ/A_V	0.4882	0.2964	0.1871	0.1159	0.04514	0.02880	0.01930	0.02962	0.03554	0.01932
NGC0024	...	231±012E−1	248±013E−1	189±012E−1	101±013E−1	683±101E−2	822±116E−2	117±016E−1	952±095E−2	120±012E−1
NGC0337	156±003E−1	193±019E−1	200±020E−1	170±017E−1	970±128E−2	665±091E−2	141±018E−1	379±047E−1	302±030E−1	677±028E−1
NGC0584	593±012E−1	908±090E−1	111±011E+0	870±087E−1	367±049E−1	219±029E−1	174±022E−1	114±014E−1	723±072E−2	481±020E−2
NGC0628	134±002E+0	164±008E+0	166±008E+0	131±007E+0	846±118E−1	546±075E−1	116±014E+0	260±033E+0	243±024E+0	324±034E+0
NGC0855	832±018E−2	898±054E−2	972±066E−2	794±067E−2	431±060E−2	281±039E−2	360±030E−2	476±057E−2	366±036E−2	854±092E−2
NGC0925	...	593±059E−1	643±064E−1	511±051E−1	310±042E−1	211±028E−1	350±044E−1	609±076E−1	564±056E−1	946±040E−1
NGC1097	...	239±023E+0	273±027E+0	228±022E+0	124±016E+0	801±109E−1	146±018E+0	318±039E+0	307±030E+0	662±027E+0
NGC1266	...	121±012E−1	126±012E−1	119±011E−1	544±074E−2	417±054E−2	545±073E−2	885±112E−2	115±011E−1	876±036E−1
NGC1291	...	436±021E+0	455±022E+0	398±020E+0	208±028E+0	127±017E+0	906±122E−1	639±079E−1	610±061E−1	481±051E−1
NGC1316	...	468±046E+0	489±048E+0	420±042E+0	248±033E+0	153±021E+0	112±014E+0	553±069E−1	623±062E−1	428±021E−1
NGC1377	...	100±010E−1	114±011E−1	944±094E−2	568±075E−2	851±117E−2	267±035E−1	420±052E−1	410±041E−1	183±007E+0
NGC1404	...	137±013E+0	159±015E+0	134±013E+0	728±098E−1	434±059E−1	331±042E−1	158±019E−1	141±014E−1	880±040E−2
IC0342	...	143±007E+1	137±006E+1	126±006E+1	142±019E+1	819±112E+0	130±016E+1	283±035E+1	252±025E+1	372±014E+1
NGC1482	...	232±023E−1	300±030E−1	293±029E−1	205±028E−1	151±020E−1	593±076E−1	155±019E+0	127±012E+0	368±014E+0
NGC1512	...	810±043E−1	855±048E−1	729±046E−1	439±052E−1	294±033E−1	260±034E−1	456±054E−1	437±043E−1	486±052E−1
NGC1566	...	138±013E+0	141±014E+0	126±012E+0	750±101E−1	479±065E−1	907±115E−1	211±026E+0	194±019E+0	283±012E+0
NGC1705	...	573±036E−2	539±044E−2	443±047E−2	266±036E−2	193±025E−2	183±019E−2	192±020E−2	200±020E−2	538±058E−2
NGC2146	...	956±048E−1	122±006E+0	110±005E+0	844±114E−1	634±087E−1	251±032E+0	681±085E+0	513±051E+0	124±004E+1
NGC2403	322±011E+0	292±014E+0	290±014E+0	238±012E+0	200±025E+0	135±017E+0	211±026E+0	387±051E+0	407±040E+0	588±063E+0
HoII	...	165±011E−1	290±019E−1	215±018E−1	774±098E−2	645±078E−2	400±047E−2	441±048E−2	430±043E−2	177±019E−1
M81dwA	...	376±038E−3	388±038E−3	292±029E−3	185±094E−3	960±960E−4	<376E−3	<236E−3	<630E−4	<173E−2
DDO053	633±043E−3	750±206E−3	137±031E−2	792±370E−3	427±100E−3	310±100E−3	264±090E−3	438±100E−3	662±068E−3	240±026E−2
NGC2798	108±002E−1	162±016E−1	185±018E−1	173±017E−1	114±015E−1	811±114E−2	265±034E−1	633±079E−1	605±060E−1	262±010E+0
NGC2841	182±003E+0	280±028E+0	321±032E+0	266±026E+0	127±017E+0	751±103E−1	669±085E−1	115±014E+0	103±010E+0	909±037E−1
NGC2915	...	125±012E−1	145±014E−1	907±090E−2	537±075E−2	347±050E−2	326±044E−2	310±039E−2	190±019E−2	628±026E−2
HoI	...	307±043E−2	395±063E−2	159±073E−2	964±141E−3	597±120E−3	374±180E−3	363±161E−3	169±084E−3	656±098E−3
NGC2976	705±014E−1	851±043E−1	887±045E−1	704±037E−1	408±059E−1	283±039E−1	515±065E−1	102±012E+0	864±086E−1	139±015E+0
NGC3049	627±014E−2	773±077E−2	816±081E−2	737±073E−2	403±052E−2	274±038E−2	652±086E−2	134±017E−1	115±011E−1	427±017E−1
NGC3031	174±005E+1	232±011E+1	252±012E+1	211±010E+1	106±014E+1	655±090E+0	558±074E+0	764±100E+0	600±060E+0	523±056E+0
NGC3034	546±018E+0	908±045E+0	106±005E+1	100±005E+1	725±227E+0	573±180E+0	236±073E+1	620±191E+1	<351E+1	324±102E+2
HoIX	141±006E−2	244±024E−2	203±020E−2	146±014E−2	736±114E−3	379±036E−3	<131E−2	<119E−2	<544E−3	<364E−2
NGC3077	890±017E−1	104±005E+0	103±005E+0	866±045E−1	537±072E−1	361±049E−1	432±054E−1	812±101E−1	773±077E−1	130±014E+0
M81dwB	110±004E−2	118±015E−2	135±022E−2	135±027E−2	539±101E−3	362±101E−3	322±090E−3	309±080E−3	387±***E−3	333±047E−3
NGC3190	437±008E−1	710±071E−1	833±083E−1	739±073E−1	372±050E−1	234±032E−1	247±031E−1	328±041E−1	286±028E−1	266±011E−1
NGC3184	769±015E−1	104±010E+0	113±011E+0	912±091E−1	557±075E−1	356±049E−1	666±084E−1	143±017E+0	119±011E+0	142±005E+0
NGC3198	424±008E−1	573±057E−1	631±063E−1	547±054E−1	273±037E−1	173±023E−1	335±042E−1	683±085E−1	623±062E−1	105±004E+0
IC2574	...	334±019E−1	230±019E−1	164±021E−1	148±020E−1	110±012E−1	643±087E−2	690±089E−2	456±046E−2	281±030E−1
NGC3265	367±009E−2	506±050E−2	572±057E−2	479±047E−2	284±037E−2	198±026E−2	411±054E−2	101±012E−1	881±088E−2	295±012E−1
Mrk33	...	490±049E−2	558±055E−2	477±047E−2	265±036E−2	189±026E−2	528±067E−2	127±016E−1	161±016E−1	862±035E−1
NGC3351	114±002E+0	167±008E+0	176±008E+0	153±007E+0	772±110E−1	501±071E−1	659±092E−1	127±016E+0	119±011E+0	253±027E+0
NGC3521	252±005E+0	370±018E+0	419±021E+0	348±017E+0	196±027E+0	129±018E+0	236±032E+0	561±076E+0	499±049E+0	549±059E+0
NGC3621	...	192±019E+0	213±021E+0	168±016E+0	992±134E−1	668±091E−1	160±020E+0	349±043E+0	304±030E+0	369±018E+0
NGC3627	245±004E+0	332±016E+0	372±018E+0	316±015E+0	178±025E+0	115±017E+0	219±030E+0	522±069E+0	475±047E+0	752±029E+0
NGC3773	357±008E−2	451±045E−2	385±038E−2	373±037E−2	222±027E−2	143±016E−2	255±034E−2	475±059E−2	421±042E−2	144±005E−1
NGC3938	476±009E−1	635±063E−1	575±057E−1	534±053E−1	321±043E−1	211±029E−1	410±052E−1	981±122E−1	871±087E−1	108±004E+0
NGC4125	...	138±013E+0	153±015E+0	128±012E+0	641±086E−1	372±050E−1	247±032E−1	143±018E−1	107±010E−1	785±042E−2
NGC4236	...	633±033E−1	829±044E−1	569±034E−1	246±033E−1	185±028E−1	184±014E−1	216±027E−1	143±014E−1	513±055E−1
NGC4254	881±017E−1	126±012E+0	134±013E+0	120±012E+0	700±094E−1	469±064E−1	149±018E+0	393±049E+0	342±034E+0	420±016E+0
NGC4321	126±002E+0	186±018E+0	200±020E+0	164±016E+0	953±128E−1	638±087E−1	121±015E+0	288±035E+0	265±026E+0	333±013E+0
NGC4450	...	120±012E+0	138±013E+0	107±010E+0	529±071E−1	325±044E−1	260±033E−1	268±033E−1	253±025E−1	209±009E−1
NGC4536	501±010E−1	711±071E−1	749±074E−1	698±069E−1	395±053E−1	286±039E−1	620±079E−1	165±020E+0	135±013E+0	346±013E+0
NGC4552	...	162±016E+0	179±017E+0	145±014E+0	828±111E−1	482±066E−1	300±038E−1	170±021E−1	103±010E−1	941±041E−2
NGC4559	558±011E−1	770±077E−1	784±078E−1	655±065E−1	353±048E−1	233±032E−1	421±053E−1	838±104E−1	648±064E−1	111±004E+0
NGC4569	115±002E+0	181±018E+0	207±020E+0	166±016E+0	763±102E−1	473±064E−1	591±075E−1	101±012E+0	961±096E−1	143±005E+0
NGC4579	117±002E+0	203±020E+0	222±022E+0	181±018E+0	867±117E−1	522±071E−1	542±069E−1	729±091E−1	728±072E−1	760±031E−1
NGC4594	556±011E+0	801±040E+0	915±045E+0	754±037E+0	391±053E+0	236±031E+0	180±022E+0	145±016E+0	113±011E+0	773±083E−1
NGC4625	815±018E−2	979±064E−2	113±008E−1	896±088E−2	487±064E−2	307±040E−2	605±076E−2	134±016E−1	115±011E−1	128±013E−1
NGC4631	123±002E+0	174±008E+0	197±010E+0	183±009E+0	119±017E+0	846±115E−1	247±031E+0	584±072E+0	477±047E+0	813±087E+0
NGC4725	161±003E+0	242±024E+0	317±031E+0	240±024E+0	113±015E+0	704±096E−1	753±095E−1	120±015E+0	901±090E−1	859±036E−1
NGC4736	530±010E+0	693±034E+0	766±038E+0	642±032E+0	344±048E+0	229±031E+0	256±034E+0	482±064E+0	467±046E+0	553±059E+0

Table 2b continued on next page

Table 2b *(continued)*

Galaxy	z	J	H	K_S	IRAC	IRAC	IRAC	IRAC	WISE	MIPS
$\lambda(\mu m)$	0.9097	1.25	1.65	2.17	3.6	4.5	5.8	8.0	12	24
A_λ/A_V	0.4882	0.2964	0.1871	0.1159	0.04514	0.02880	0.01930	0.02962	0.03554	0.01932
DDO154	125±005E−2	991±262E−3	124±039E−2	119±047E−2	511±100E−3	350±100E−3	<403E−3	<399E−3	<124E−3	<438E−3
NGC4826	353±007E+0	564±028E+0	628±031E+0	526±026E+0	240±034E+0	151±021E+0	160±021E+0	224±029E+0	191±019E+0	255±027E+0
DDO165	320±009E−2	318±036E−2	468±055E−2	372±062E−2	127±023E−2	909±150E−3	588±170E−3	408±080E−3	<168E−3	<449E−3
NGC5033	···	120±012E+0	134±013E+0	116±011E+0	640±086E−1	470±064E−1	815±103E−1	192±023E+0	177±017E+0	197±007E+0
NGC5055	315±006E+0	420±021E+0	495±024E+0	404±020E+0	237±032E+0	155±021E+0	259±033E+0	558±070E+0	540±054E+0	559±060E+0
NGC5194	300±010E+0	496±024E+0	586±029E+0	451±022E+0	266±036E+0	179±025E+0	423±053E+0	106±013E+1	104±010E+1	124±013E+1
NGC5195	149±005E+0	235±011E+0	278±013E+0	225±011E+0	833±113E−1	511±070E−1	462±060E−1	646±080E−1	102±010E+0	146±015E+0
NGC5398	···	805±080E−2	664±066E−2	537±053E−2	377±050E−2	246±036E−2	144±020E−2	587±075E−2	663±066E−2	279±013E−1
NGC5457	391±007E+0	437±022E+0	503±025E+0	441±022E+0	281±038E+0	189±026E+0	339±042E+0	761±094E+0	706±070E+0	105±011E+1
NGC5408	···	185±018E−1	165±016E−1	108±010E−1	514±072E−2	369±051E−2	412±053E−2	377±047E−2	668±066E−2	428±017E−1
NGC5474	225±004E−1	143±009E−1	158±012E−1	113±013E−1	109±013E−1	731±102E−2	555±101E−2	114±014E−1	103±010E−1	156±016E−1
NGC5713	242±004E−1	373±037E−1	386±038E−1	331±033E−1	201±027E−1	137±019E−1	289±037E−1	114±014E+0	101±010E+0	234±009E+0
NGC5866	903±018E−1	130±013E+0	148±014E+0	126±012E+0	663±089E−1	420±057E−1	312±039E−1	314±039E−1	268±026E−1	214±009E−1
IC4710	···	106±010E−1	990±099E−2	772±077E−2	699±097E−2	464±064E−2	450±061E−2	648±083E−2	375±037E−2	118±005E−1
NGC6822	···	552±055E+0	553±055E+0	420±042E+0	210±028E+0	137±018E+0	144±018E+0	140±017E+0	116±011E+0	317±012E+0
NGC6946	···	701±070E+0	531±053E+0	553±055E+0	328±044E+0	217±029E+0	585±073E+0	140±017E+1	135±013E+1	203±008E+1
NGC7331	189±003E+0	282±028E+0	333±033E+0	280±028E+0	160±021E+0	101±014E+0	186±023E+0	404±050E+0	347±034E+0	436±024E+0
NGC7552	···	706±070E−1	796±079E−1	697±069E−1	453±061E−1	360±049E−1	106±013E+0	270±033E+0	273±027E+0	106±004E+1
NGC7793	···	167±008E+0	169±008E+0	130±006E+0	746±104E−1	481±064E−1	104±013E+0	189±023E+0	151±015E+0	209±022E+0

NOTE—The compact table entry format TUV±WXYEZ implies (T.UV±W.XY)×10^Z in Jy. Corrections for neither Galactic nor intrinsic extinction has been applied (see § 3). The uncertainties include both statistical and systematic effects. 5σ upper limits are provided for non-detections. No color corrections have been applied.

c

Table 2c. Global Flux Densities in Janskys Corrected for Neither Galactic Nor Intrinsic Extinction

Galaxy	MIPS	PACS	PACS	MIPS	PACS	SPIRE	SPIRE	SPIRE	SCUBA	VLA
$\lambda(\mu m)$	70	70	100	160	160	250	350	500	850	20 cm
A_λ/A_V	0.002308	0.002308	0.001037	0.000388	0.000388	0.0001521	0.0000725	0.00003605	0.00001458	0.0
NGC0024	222±027E+0	...	...	712±111E+0	...	...	...	...	...	...
NGC0337	111±013E+1	139±006E+1	210±010E+1	200±025E+1	197±009E+1	902±064E+0	409±029E+0	162±011E+0	349±052E−1	109±010E−1
NGC0584	175±498E−1	180±025E−1	300±033E−1	118±050E+0	610±038E−1	<887E−1	<603E−1	<419E−1	...	<500E−2
NGC0628	338±041E+1	421±021E+1	837±041E+1	111±017E+2	114±005E+2	626±044E+1	301±021E+1	116±008E+1	...	172±017E−1
NGC0855	168±020E+0	208±010E+0	253±013E+0	222±034E+0	206±010E+0	137±009E+0	734±053E−1	226±018E−1	...	490±050E−3
NGC0925	143±019E+1	136±006E+1	289±014E+1	433±054E+1	372±018E+1	253±017E+1	139±009E+1	665±047E+0	...	460±050E−2
NGC1097	598±053E+1	787±039E+1	123±006E+2	153±018E+2	132±006E+2	674±047E+1	296±021E+1	109±007E+1	144±078E+0	414±041E−1
NGC1266	126±015E+1	149±007E+1	171±008E+1	102±014E+1	113±005E+1	408±029E+0	147±010E+0	410±031E−1	...	116±012E−1
NGC1291	527±064E+0	439±027E+0	135±007E+1	262±041E+1	226±011E+1	152±010E+1	766±054E+0	316±022E+0	...	...
NGC1316	544±126E+0	568±029E+0	997±050E+0	126±019E+1	124±006E+1	499±035E+0	206±015E+0	721±059E−1	...	255±026E−1
NGC1377	634±095E+0	725±036E+0	651±032E+0	338±056E+0	337±016E+0	123±008E+0	474±034E−1	167±013E−1	...	<100E−3
NGC1404	<165E−1	<214E−1	<252E−1	<286E−1	<204E−1	<163E−1	<134E−1	<909E−2	...	390±060E−3
IC0342	352±024E+2	471±023E+2	895±044E+2	915±109E+2	107±005E+3	569±040E+2	254±018E+2	941±066E+1	...	240±024E+0
NGC1482	324±034E+1	419±020E+1	522±026E+1	387±048E+1	419±021E+1	155±011E+1	588±041E+0	180±012E+0	330±050E−1	238±024E−1
NGC1512	682±083E+0	752±039E+0	150±007E+1	196±030E+1	191±009E+1	148±010E+1	875±062E+0	371±027E+0	...	700±100E−3
NGC1566	343±032E+1	...	...	102±012E+2	...	...	...	...	...	400±000E−1
NGC1705	124±015E+0	...	...	139±021E+0	...	...	...	...	...	...
NGC2146	215±015E+2	198±009E+2	236±011E+2	119±014E+2	174±008E+2	618±043E+1	223±015E+1	695±049E+0	...	107±010E+0
NGC2403	857±104E+1	...	...	225±035E+2	...	...	...	...	...	330±033E−1
HoII	318±039E+0	438±022E+0	574±028E+0	346±054E+0	363±018E+0	154±011E+0	779±067E−1	289±144E−1	...	197±028E−2
M81dwA	<149E−1	...	...	<143E−1	...	...	...	...	...	...
DDO053	315±040E−1	400±025E−1	520±031E−1	357±061E−1	300±020E−1	140±014E−1	100±010E−1	<389E−2	...	...
NGC2798	217±023E+1	250±012E+1	287±014E+1	206±026E+1	202±010E+1	746±053E+0	275±019E+0	870±062E−1	194±032E−1	829±085E−2
NGC2841	102±014E+1	110±005E+1	286±014E+1	622±076E+1	488±024E+1	324±023E+1	154±010E+1	600±042E+0	...	840±086E−2
NGC2915	140±047E+0	107±005E+0	180±009E+0	145±041E+0	162±008E+0	823±059E−1	468±034E−1	209±016E−1	...	...
HoI	292±040E−1	401±033E−1	441±039E−1	526±092E−1	432±034E−1	372±031E−1	231±020E−1	110±012E−1	...	...
NGC2976	199±024E+1	209±010E+1	372±018E+1	426±066E+1	459±022E+1	244±017E+1	114±008E+1	451±032E+0	609±236E−1	508±054E−2
NGC3049	289±072E+0	382±019E+0	529±026E+0	486±072E+0	494±024E+0	261±018E+0	132±009E+0	657±047E−1	...	120±023E−2
NGC3031	852±104E+1	...	...	308±048E+2	...	...	...	...	...	379±037E−1
NGC3034	162±051E+3	...	...	857±271E+2	...	...	...	...	551±082E+0	765±077E+0
HoIX	<228E−1	...	...	<457E−1	...	...	...	...	...	...
NGC3077	196±024E+1	213±010E+1	293±014E+1	281±043E+1	278±013E+1	133±009E+1	620±044E+0	242±017E+0	...	...
M81dwB	114±016E−1	904±116E−2	270±018E−1	161±031E−1	292±018E−1	178±014E−1	105±010E−1	435±217E−2	...	...
NGC3190	565±094E+0	629±031E+0	109±005E+1	150±019E+1	153±007E+1	826±058E+0	352±025E+0	121±008E+0	189±035E−1	430±047E−2
NGC3184	157±020E+1	180±009E+1	392±019E+1	704±086E+1	537±026E+1	317±022E+1	148±010E+1	589±042E+0	...	559±059E−2
NGC3198	102±013E+1	109±005E+1	224±011E+1	389±050E+1	296±014E+1	183±013E+1	965±068E+0	412±029E+0	...	270±034E−2
IC2574	483±059E+0	578±029E+0	937±047E+0	105±016E+1	986±049E+0	574±041E+0	417±029E+0	169±012E+0	...	107±023E−2
NGC3265	270±066E+0	292±014E+0	322±016E+0	270±047E+0	285±014E+0	116±008E+0	514±037E−1	198±016E−1	...	111±023E−2
Mrk33	434±081E+0	...	...	386±060E+0	...	...	...	...	400±060E−2	172±026E−2
NGC3351	218±026E+1	270±013E+1	486±024E+1	569±088E+1	538±026E+1	316±022E+1	139±009E+1	490±034E+0	...	438±048E−2
NGC3521	644±078E+1	800±040E+1	163±008E+2	195±030E+2	203±010E+2	107±007E+2	464±032E+1	168±011E+1	210±082E+0	356±035E−1
NGC3621	501±046E+1	504±025E+1	101±005E+2	139±017E+2	124±006E+2	654±046E+1	308±021E+1	125±008E+1	...	197±019E−1
NGC3627	919±070E+1	107±005E+2	188±009E+2	215±027E+2	196±009E+2	912±064E+1	364±025E+1	123±008E+1	186±070E+0	457±045E−1
NGC3773	157±052E+0	139±007E+0	214±010E+0	238±048E+0	206±010E+0	953±068E−1	419±030E−1	158±012E−1	...	580±050E−3
NGC3938	142±017E+1	164±008E+1	307±015E+1	519±063E+1	392±019E+1	221±015E+1	993±070E+0	373±026E+0	...	617±065E−2
NGC4125	111±052E+0	...	...	176±042E+0	...	...	...	...	...	<500E−2
NGC4236	802±098E+0	803±041E+0	113±005E+1	161±025E+1	172±008E+1	107±007E+1	702±050E+0	364±026E+0	...	281±034E−2
NGC4254	502±043E+1	596±029E+1	110±005E+2	142±017E+2	126±006E+2	623±044E+1	252±017E+1	849±060E+0	100±054E+0	421±041E−1
NGC4321	405±037E+1	440±022E+1	907±045E+1	139±016E+2	116±005E+2	632±044E+1	268±019E+1	919±065E+0	875±493E−1	340±034E−1
NGC4450	342±108E+0	...	...	169±022E+1	...	...	...	...	...	940±100E−3
NGC4536	319±031E+1	419±020E+1	567±028E+1	580±071E+1	555±027E+1	270±019E+1	122±008E+1	471±033E+0	414±112E−1	194±018E−1
NGC4552	537±778E−1	...	...	142±073E+0	...	...	...	...	...	100±003E−1
NGC4559	168±019E+1	180±009E+1	337±016E+1	541±066E+1	405±020E+1	238±016E+1	123±008E+1	540±038E+0	...	654±068E−2
NGC4569	123±015E+1	148±007E+1	325±016E+1	412±052E+1	400±020E+1	210±014E+1	909±064E+0	315±022E+0	464±082E−1	834±086E−2
NGC4579	953±140E+0	100±005E+1	254±012E+1	410±050E+1	345±017E+1	196±013E+1	852±060E+0	303±021E+0	439±066E−1	984±100E−2
NGC4594	730±089E+0	808±041E+0	259±013E+1	406±063E+1	380±019E+1	240±017E+1	117±008E+1	487±034E+0	372±108E−1	136±014E−1
NGC4625	185±022E+0	151±008E+0	376±019E+0	508±079E+0	469±023E+0	258±018E+0	131±009E+0	560±041E−1	...	710±210E−3
NGC4631	138±016E+2	140±007E+2	233±011E+2	269±042E+2	238±011E+2	115±008E+2	529±037E+1	205±014E+1	573±120E+0	120±012E+0
NGC4725	885±140E+0	103±005E+1	260±013E+1	599±074E+1	466±023E+1	305±021E+1	162±011E+1	661±047E+0	...	280±034E−2
NGC4736	100±012E+2	107±005E+2	165±008E+2	164±025E+2	141±007E+2	640±045E+1	263±018E+1	920±065E+0	153±065E+0	270±027E−1

Table 2c continued on next page

Table 2c *(continued)*

Galaxy	MIPS	PACS	PACS	MIPS	PACS	SPIRE	SPIRE	SPIRE	SCUBA	VLA
$\lambda(\mu m)$	70	70	100	160	160	250	350	500	850	20 cm
A_λ/A_V	0.002308	0.002308	0.001037	0.000388	0.000388	0.0001521	0.0000725	0.00003605	0.00001458	0.0
DDO154	<591E−2	<775E−2	<912E−2	<223E−1	<801E−2	<544E−2	<483E−2	<349E−2	···	···
NGC4826	528±064E+1	563±028E+1	975±048E+1	857±133E+1	906±045E+1	396±028E+1	158±011E+1	527±037E+0	123±030E+0	101±009E−1
DDO165	<141E−1	<976E−2	<119E−1	<205E−1	<101E−1	<807E−2	<713E−2	<484E−2	···	···
NGC5033	288±028E+1	···	···	910±112E+1	···	···	···	···	109±055E+0	178±017E−1
NGC5055	744±090E+1	764±038E+1	175±008E+2	273±042E+2	241±012E+2	139±009E+2	617±043E+1	225±016E+1	···	389±039E−1
NGC5194	156±019E+2	···	···	477±074E+2	···	···	···	···	261±039E+0	149±015E+0
NGC5195	972±118E+0	···	···	129±020E+1	···	···	···	···	259±039E−1	495±053E−2
NGC5398	203±059E+0	245±012E+0	333±016E+0	351±065E+0	283±014E+0	188±013E+0	102±007E+0	499±036E−1	···	420±080E−3
NGC5457	118±014E+2	135±006E+2	262±013E+2	399±062E+2	336±016E+2	195±013E+2	952±067E+1	396±028E+1	···	749±075E−1
NGC5408	358±075E+0	369±018E+0	275±014E+0	256±052E+0	231±011E+0	829±061E−1	420±032E−1	150±014E−1	···	···
NGC5474	347±042E+0	354±018E+0	604±031E+0	913±142E+0	853±043E+0	486±034E+0	283±020E+0	136±009E+0	···	120±023E−2
NGC5713	236±024E+1	295±014E+1	421±021E+1	396±049E+1	385±019E+1	157±011E+1	615±043E+0	197±014E+0	572±119E−1	159±016E−1
NGC5866	870±120E+0	880±044E+0	180±009E+1	177±022E+1	178±008E+1	764±054E+0	308±022E+0	984±073E−1	140±020E−1	227±030E−2
IC4710	237±074E+0	···	···	356±065E+0	···	···	···	···	···	···
NGC6822	637±061E+1	···	···	143±017E+2	···	···	···	···	···	694±140E−2
NGC6946	207±016E+2	252±012E+2	457±022E+2	502±060E+2	525±026E+2	258±018E+2	107±007E+2	369±026E+1	298±044E+0	139±014E+0
NGC7331	749±073E+1	688±034E+1	135±006E+2	189±024E+2	171±008E+2	890±063E+1	389±027E+1	142±010E+1	211±038E+0	372±037E−1
NGC7552	675±114E+1	···	···	933±113E+1	···	···	···	···	795±166E−1	275±028E−1
NGC7793	329±040E+1	350±017E+1	695±034E+1	107±016E+2	901±045E+1	531±037E+1	279±019E+1	120±008E+1	···	102±009E−1

NOTE—The compact table entry format TUV±WXYEZ implies (T.UV±W.XY)×10^{Z} in Jy. Corrections for neither Galactic nor intrinsic extinction has been applied (see § 3). The uncertainties include both statistical and systematic effects. 5σ upper limits are provided for non-detections. No color corrections have been applied.

Table 3. Optical $BVR_{\rm C}I_{\rm C}$ Photometry Source

Galaxy	B	V	$R_{\rm C}$	$I_{\rm C}$
NGC0024	PS1	PS1	PS1	PS1
NGC0337	PS1	PS1	PS1	PS1
NGC0584	PS1	PS1	PS1	PS1
NGC0628	PS1	PS1	PS1	PS1
NGC0855	RC3	RC3	C14	···
NGC0925	PS1	PS1	PS1	PS1
NGC1097	MM09	MM09	MM09	MM09
NGC1266	PS1	PS1	PS1	PS1
NGC1291	MM09	MM09	MM09	MM09
NGC1316	MM09	MM09	MM09	MM09
NGC1377	PS1	PS1	PS1	PS1
NGC1404	MM09	MM09	MM09	MM09
IC0342	RC3	···	···	···
NGC1482	PS1	PS1	PS1	PS1
NGC1512	MM09	MM09	MM09	MM09
NGC1566	MM09	MM09	MM09	MM09
NGC1705	MM09	MM09	MM09	MM09
NGC2403	PS1	PS1	PS1	PS1
NGC2146	RC3	RC3	···	T09
HolmbII	PS1	PS1	PS1	PS1
M81dwA	PS1	PS1	PS1	PS1
DDO053	PS1	PS1	PS1	PS1
NGC2798	PS1	PS1	PS1	PS1
NGC2841	PS1	PS1	PS1	PS1
NGC2915	RC3	MM09	MM09	D07
HolmbI	PS1	PS1	PS1	PS1
NGC2976	PS1	PS1	PS1	PS1
NGC3049	PS1	PS1	PS1	PS1
NGC3031	RC3	RC3	···	T09
NGC3034	PS1	PS1	PS1	PS1
HolmbIX	PS1	PS1	PS1	PS1
NGC3077	C14	···	RC3	···
M81dwB	PS1	PS1	PS1	PS1
NGC3190	PS1	PS1	PS1	PS1
NGC3184	PS1	PS1	PS1	PS1
NGC3198	PS1	PS1	PS1	PS1
IC2574	PS1	PS1	PS1	PS1
NGC3265	PS1	PS1	PS1	PS1
Mrk33	PS1	PS1	PS1	PS1
NGC3351	PS1	PS1	PS1	PS1
NGC3521	PS1	PS1	PS1	PS1
NGC3621	MM09	MM09	MM09	MM09
NGC3627	PS1	PS1	PS1	PS1
NGC3773	PS1	PS1	PS1	PS1
NGC3938	PS1	PS1	PS1	PS1
NGC4125	PS1	PS1	PS1	PS1
NGC4236	PS1	PS1	PS1	PS1
NGC4254	PS1	PS1	PS1	PS1
NGC4321	PS1	PS1	PS1	PS1

Table 3 continued on next page

Table 3 *(continued)*

Galaxy	B	V	R_C	I_C
NGC4450	PS1	PS1	PS1	PS1
NGC4536	PS1	PS1	PS1	PS1
NGC4552	PS1	PS1	PS1	PS1
NGC4559	PS1	PS1	PS1	PS1
NGC4569	RC3	RC3	···	···
NGC4579	PS1	PS1	PS1	PS1
NGC4594	PS1	PS1	PS1	PS1
NGC4625	PS1	PS1	PS1	PS1
NGC4631	PS1	PS1	PS1	PS1
NGC4725	PS1	PS1	PS1	PS1
NGC4736	PS1	PS1	PS1	PS1
DDO154	PS1	PS1	PS1	PS1
NGC4826	PS1	PS1	PS1	PS1
DDO165	PS1	PS1	PS1	PS1
NGC5033	PS1	PS1	···	PS1
NGC5055	RC3	RC3	C14	T09
NGC5194	PS1	PS1	PS1	PS1
NGC5195	PS1	PS1	PS1	PS1
NGC5398	D07	D07	D07	D07
NGC5457	RC3	RC3	C14	T09
NGC5408	RC3	RC3	···	···
NGC5474	PS1	PS1	PS1	PS1
NGC5713	PS1	PS1	PS1	PS1
NGC5866	PS1	PS1	PS1	PS1
IC4710	D07	D07	D07	···
NGC6822	PS1	PS1	PS1	PS1
NGC6946	RC3	PS1	···	PS1
NGC7331	PS1	PS1	PS1	PS1
NGC7552	MM09	MM09	D07	D07
NGC7793	D07	D07	D07	D07

NOTE—PS1: recalibration of Dale et al. (2007) photometry using Pan-STARRS1 (§3.1); D07: Dale et al. (2007); MM09: Muñoz-Mateos et al. (2009); C14: Cook et al. (2014); T09: unpublished photometry from M. Pierce via the Extragalactic Distance Database (Tully et al. 2009); RC3: de Vaucouleurs et al. (1991).

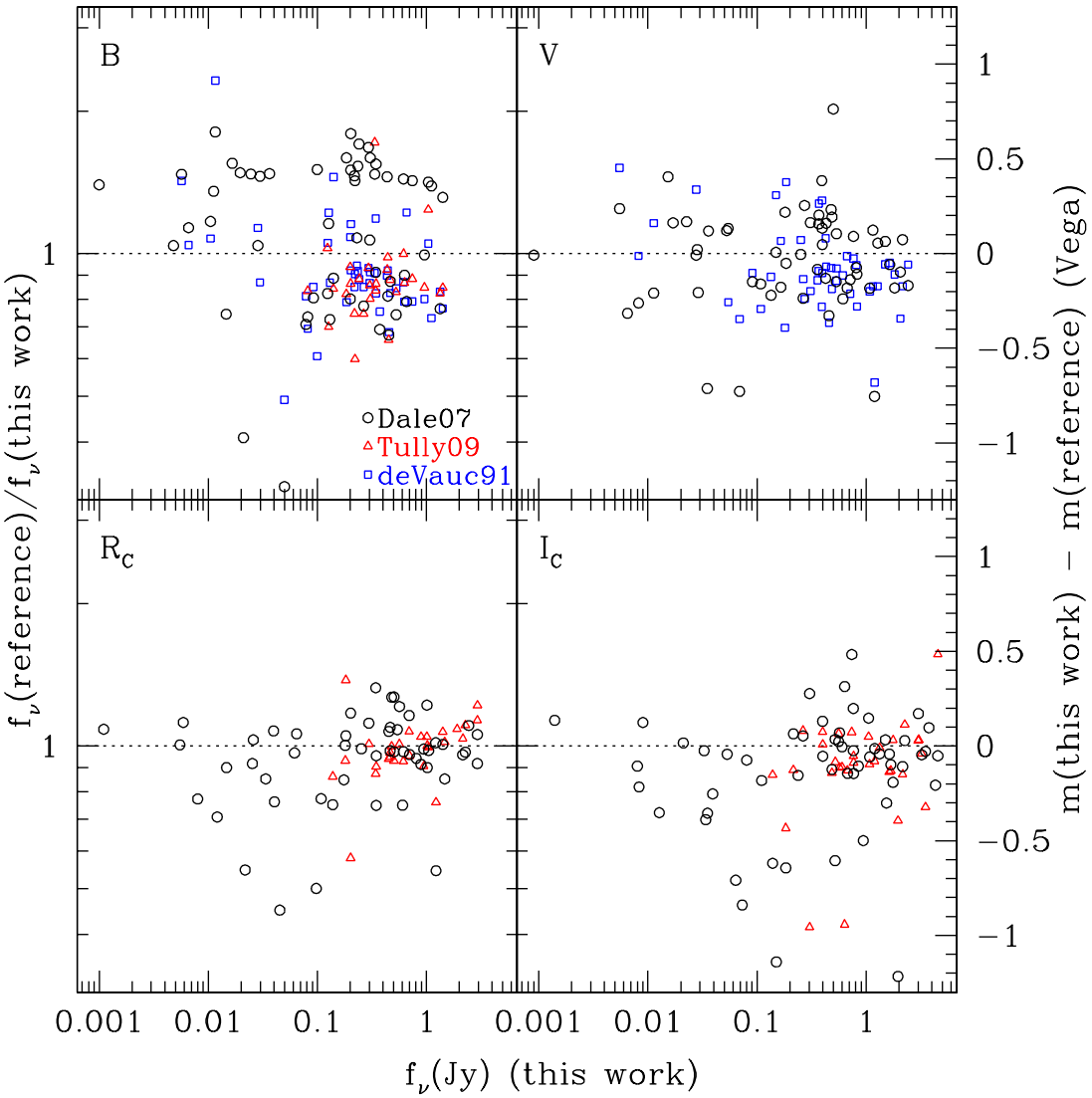

Figure 1. Comparison of global BVR_CI_C galaxy photometry from the literature with those measured here which are calibrated based on Pan-STARRS1 $g_{P1}r_{P1}i_{P1}z_{P1}$ photometry on field stars (see § 3.1).

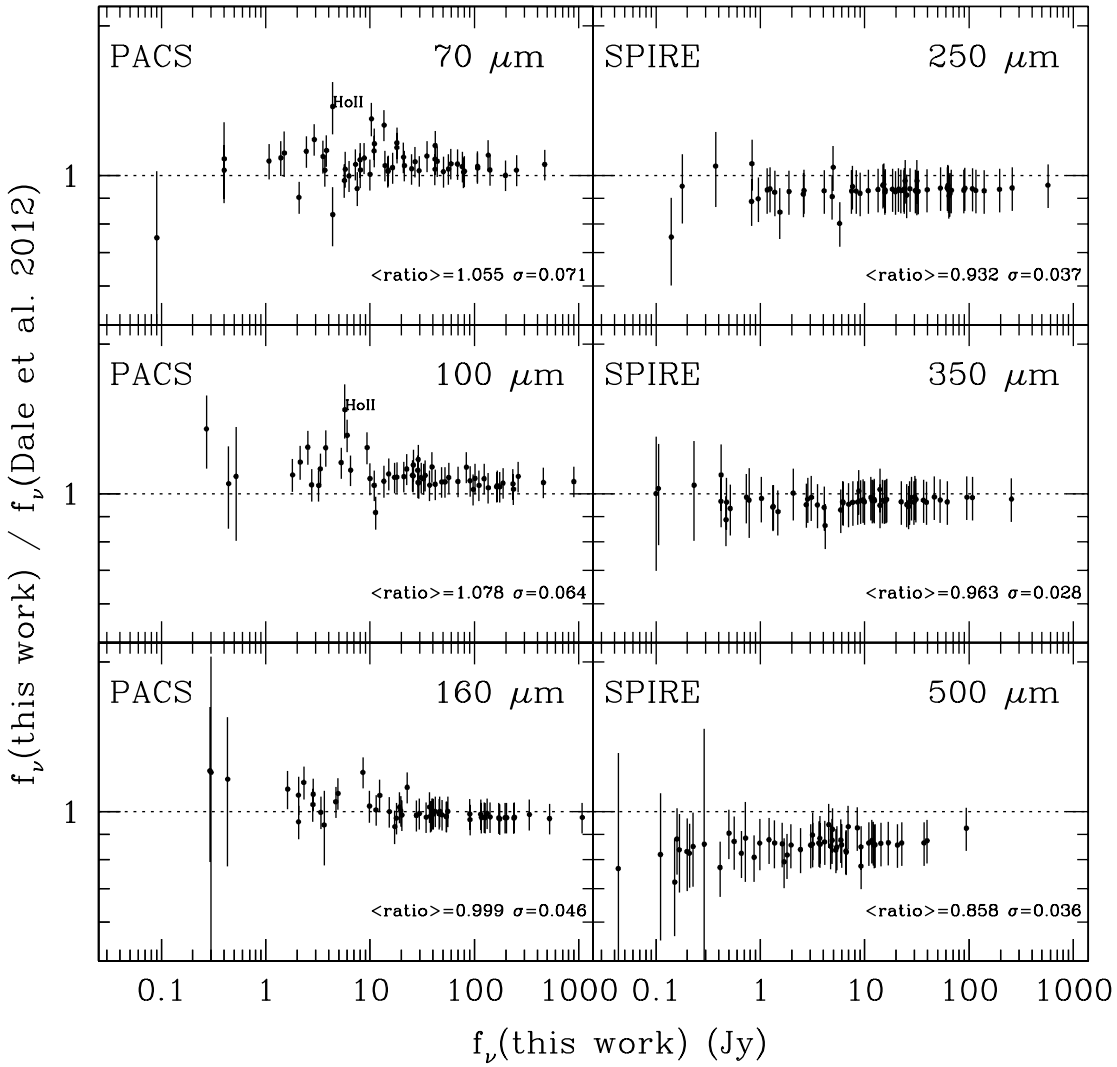

Figure 2. Comparison of updated global *Herschel* photometry with those presented in Dale et al. (2012).

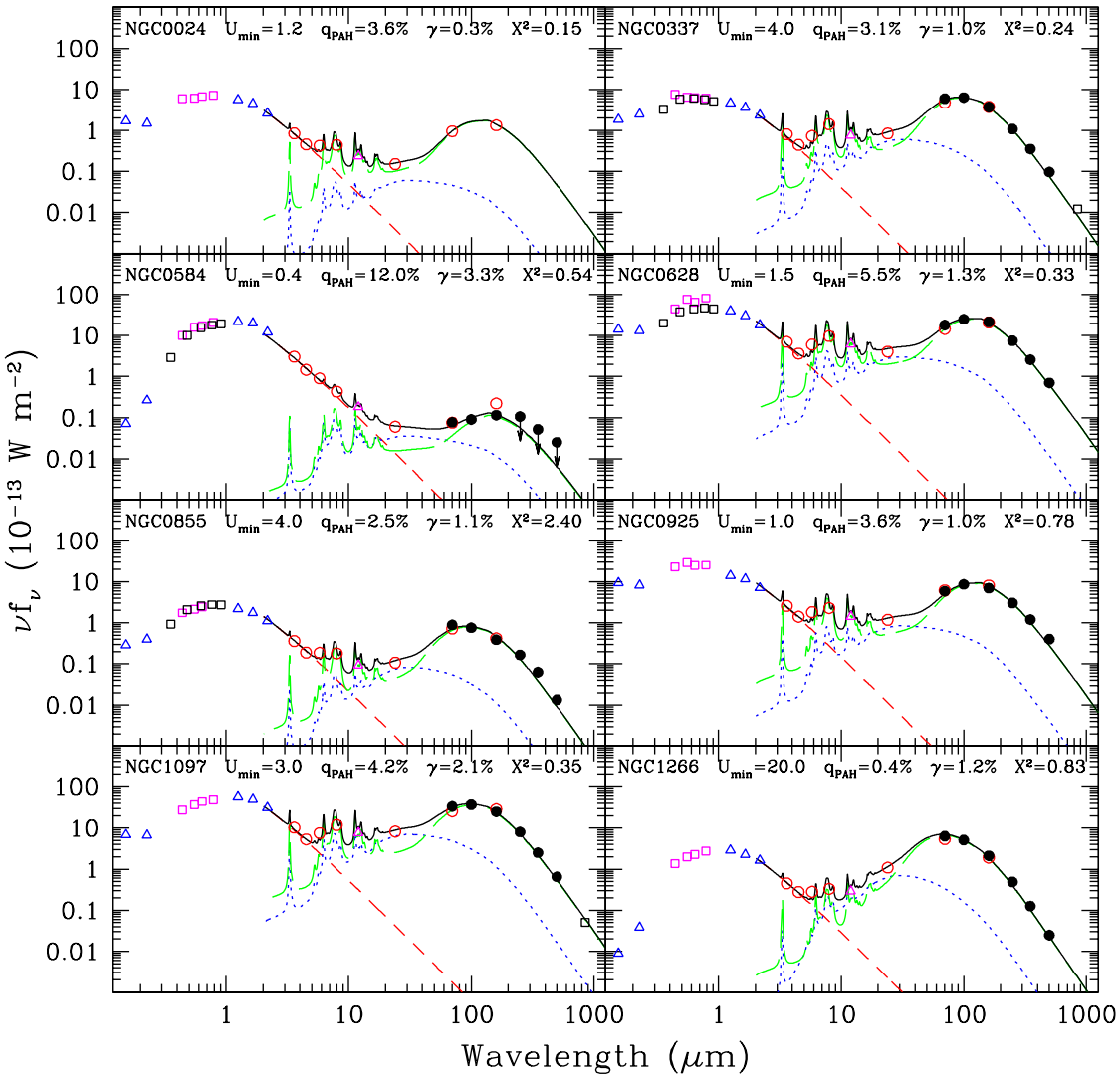

Figure 3. Globally-integrated infrared/sub-millimeter spectral energy distributions for all the galaxies in the KINGFISH sample, sorted by Right Ascension. The following symbols are utilized: filled circles (*Herschel*), triangles (*GALEX*, *2MASS*, and *WISE*), open circles (*Spitzer*), squares (BVR_CI_C and *ugriz* and SCUBA). Arrows indicate 5σ upper limits (and lower limits in the case of NGC 3034). The solid curve is the sum of a 5000 K stellar blackbody (short dashed) along with models of dust emission from PDRs (dotted; $U > U_{\rm min}$) and the diffuse interstellar medium (long dashed; $U = U_{\rm min}$). The fitted parameters from these Draine & Li (2007) model fits are listed within each panel along with the reduced χ^2 (see § 4.4 for details). While the plotted data are corrected for Galactic extinction, the fluxes tabulated in Table **??** are not corrected.

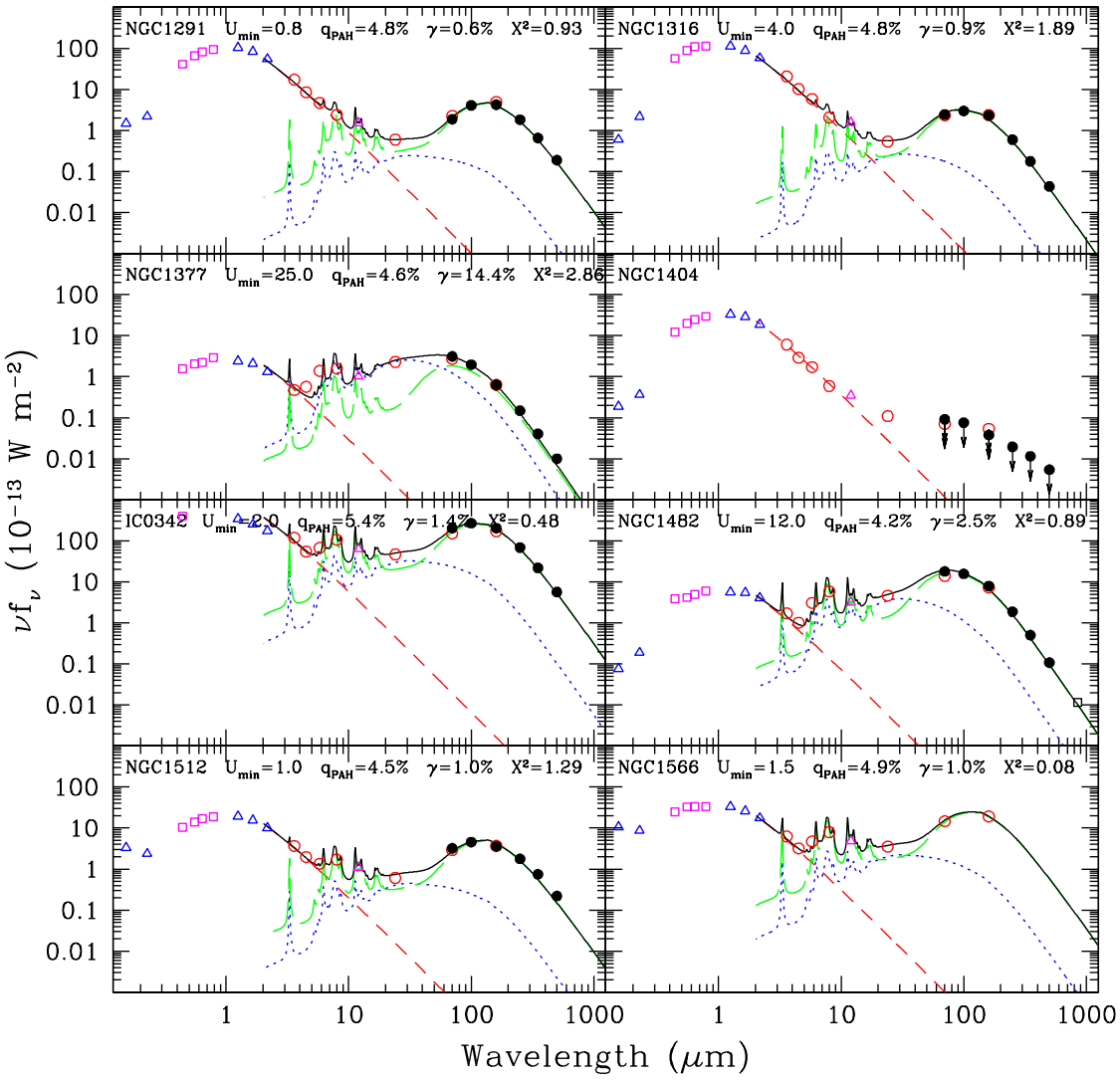

Figure 3. Globally-integrated infrared/sub-millimeter spectral energy distributions for the KINGFISH sample (continued).

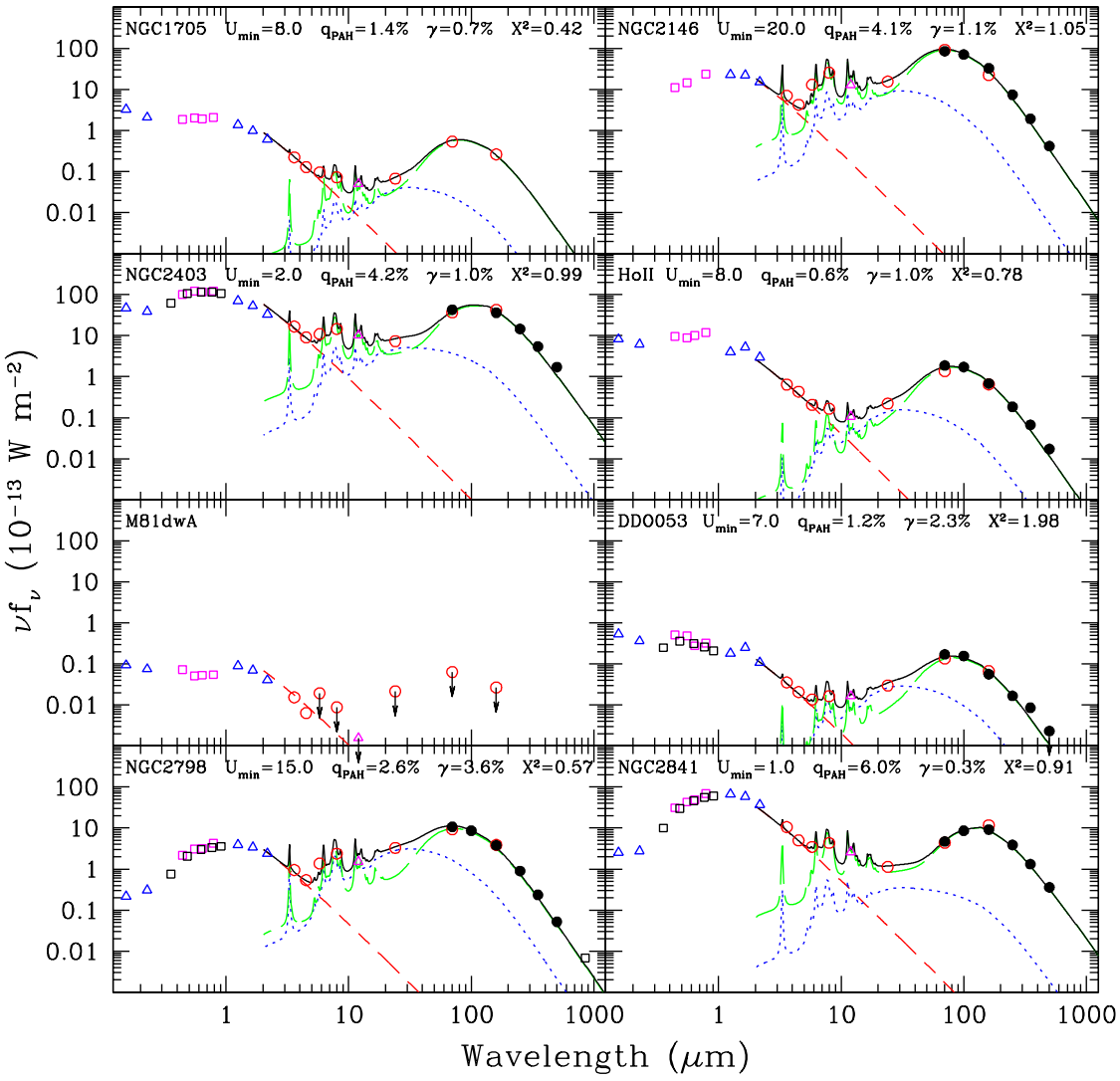

Figure 3. Globally-integrated infrared/sub-millimeter spectral energy distributions for the KINGFISH sample (continued).

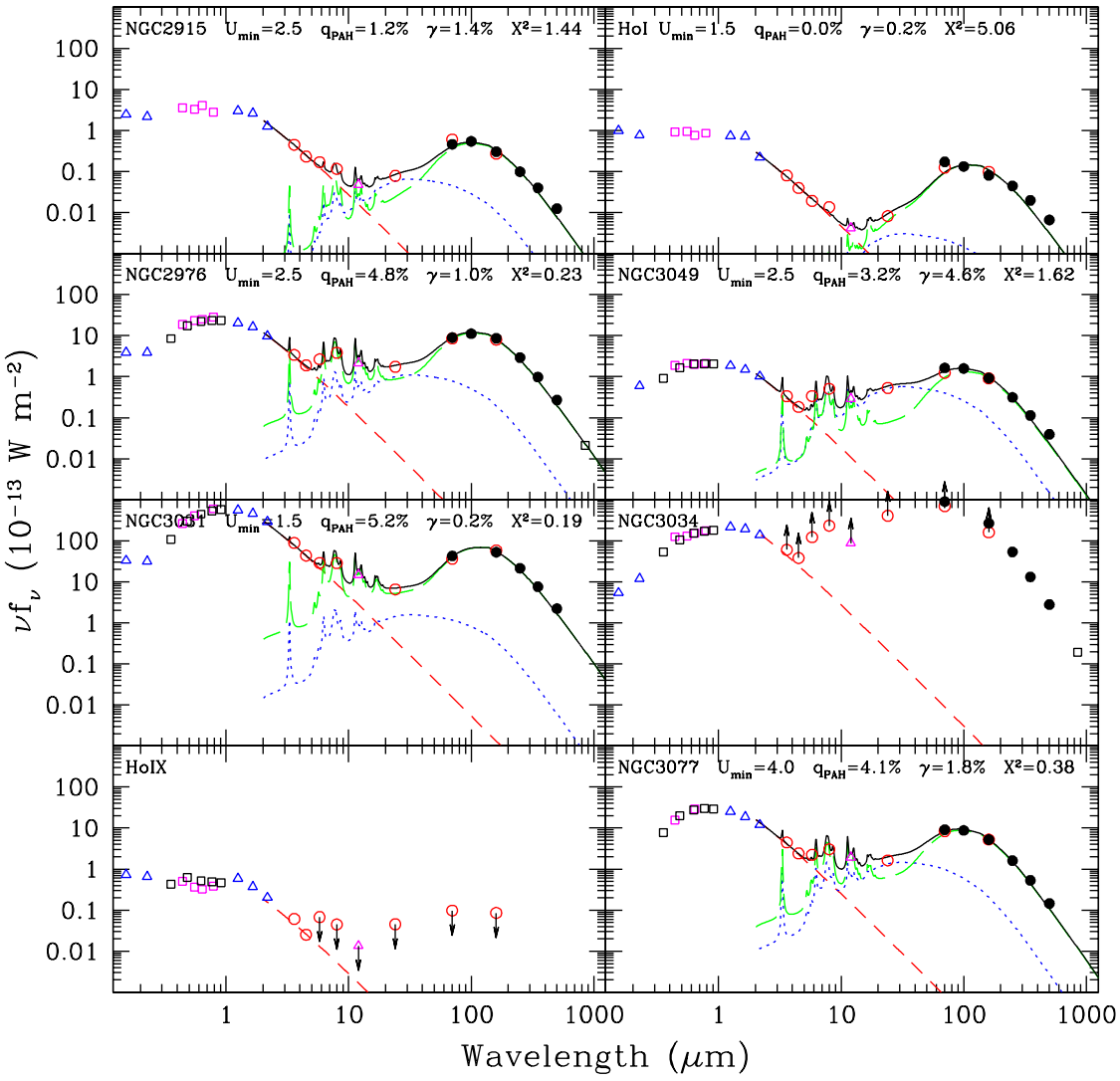

Figure 3. Globally-integrated infrared/sub-millimeter spectral energy distributions for the KINGFISH sample (continued).

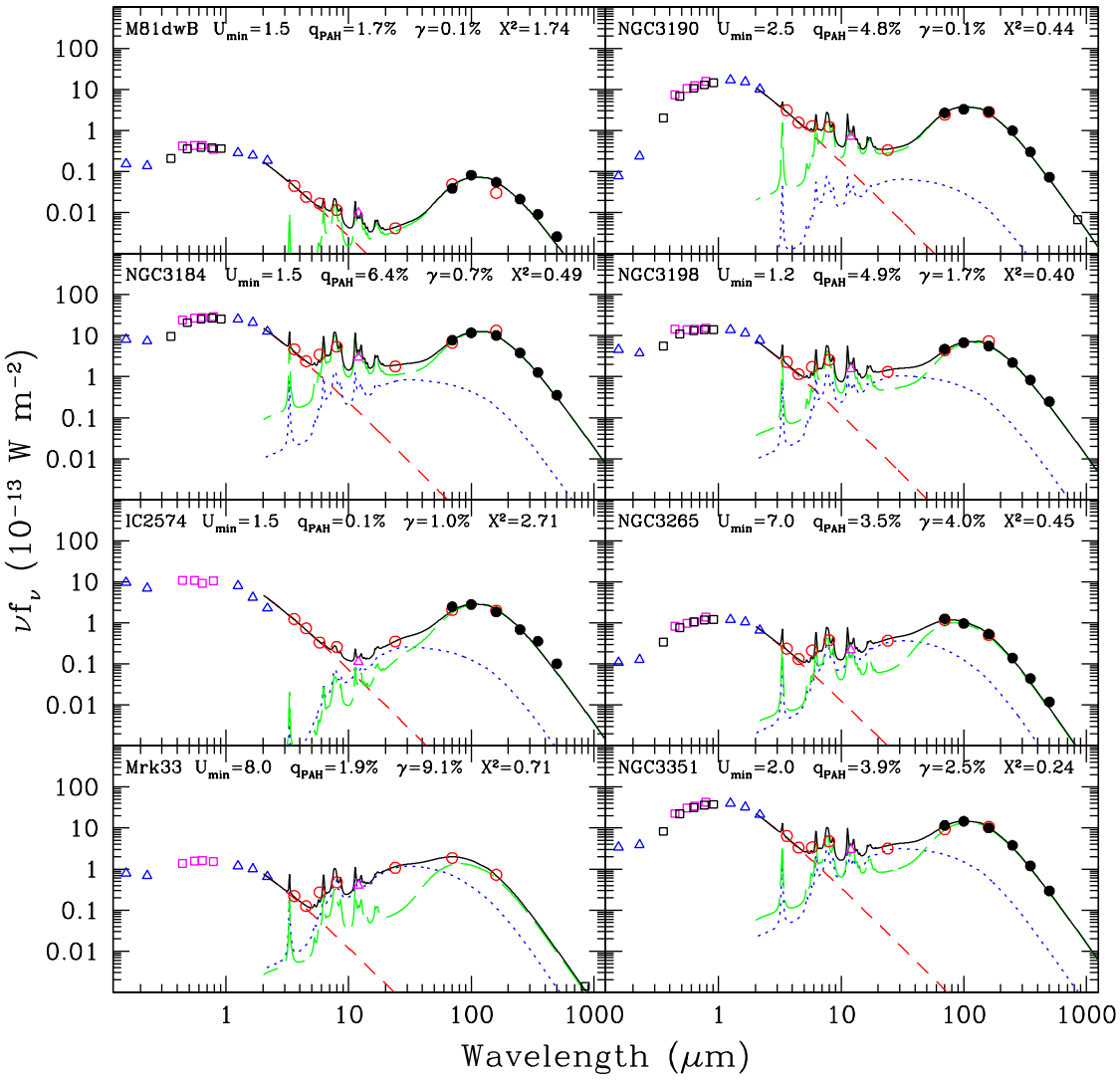

Figure 3. Globally-integrated infrared/sub-millimeter spectral energy distributions for the KINGFISH sample (continued).

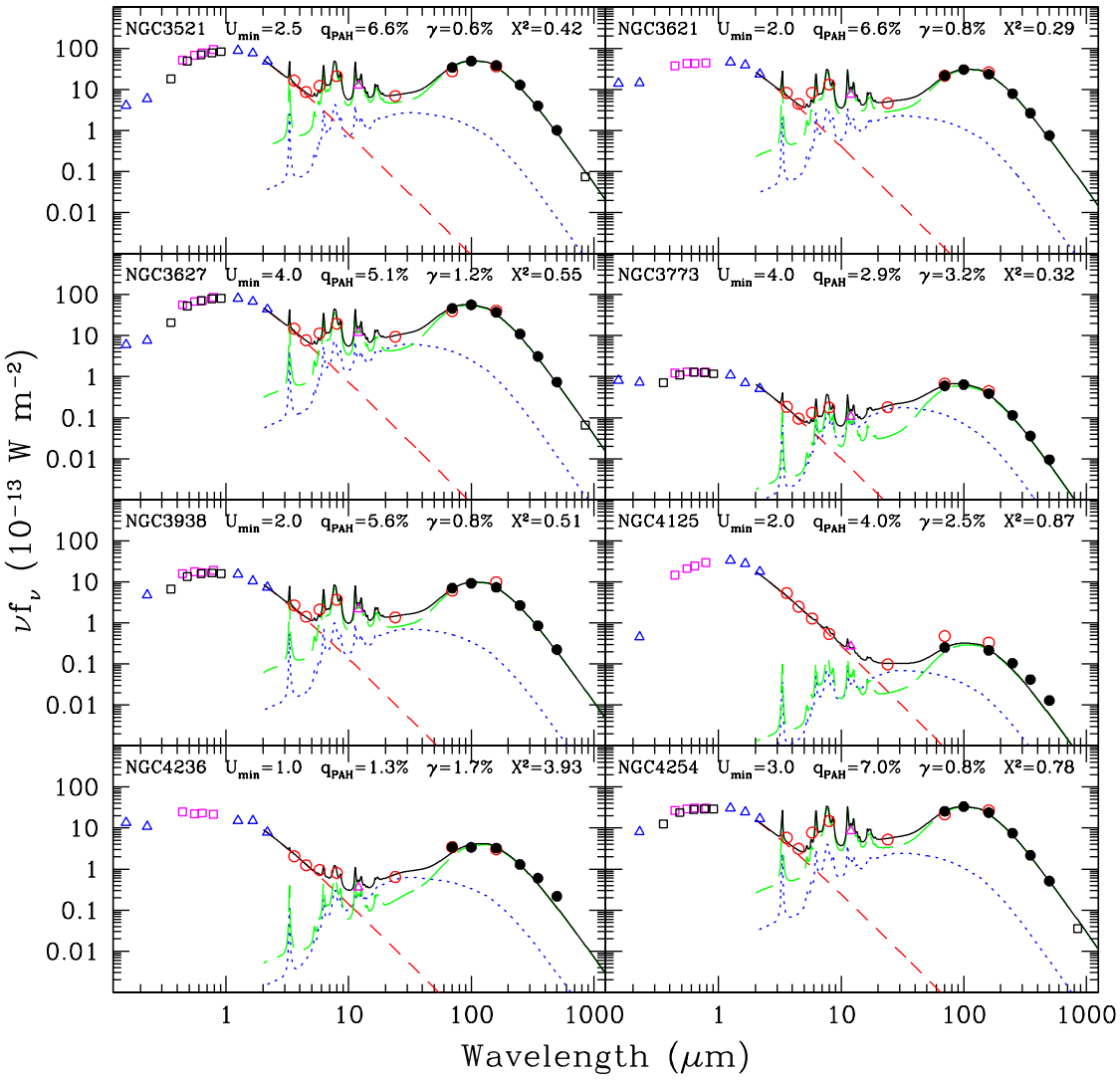

Figure 3. Globally-integrated infrared/sub-millimeter spectral energy distributions for the KINGFISH sample (continued).

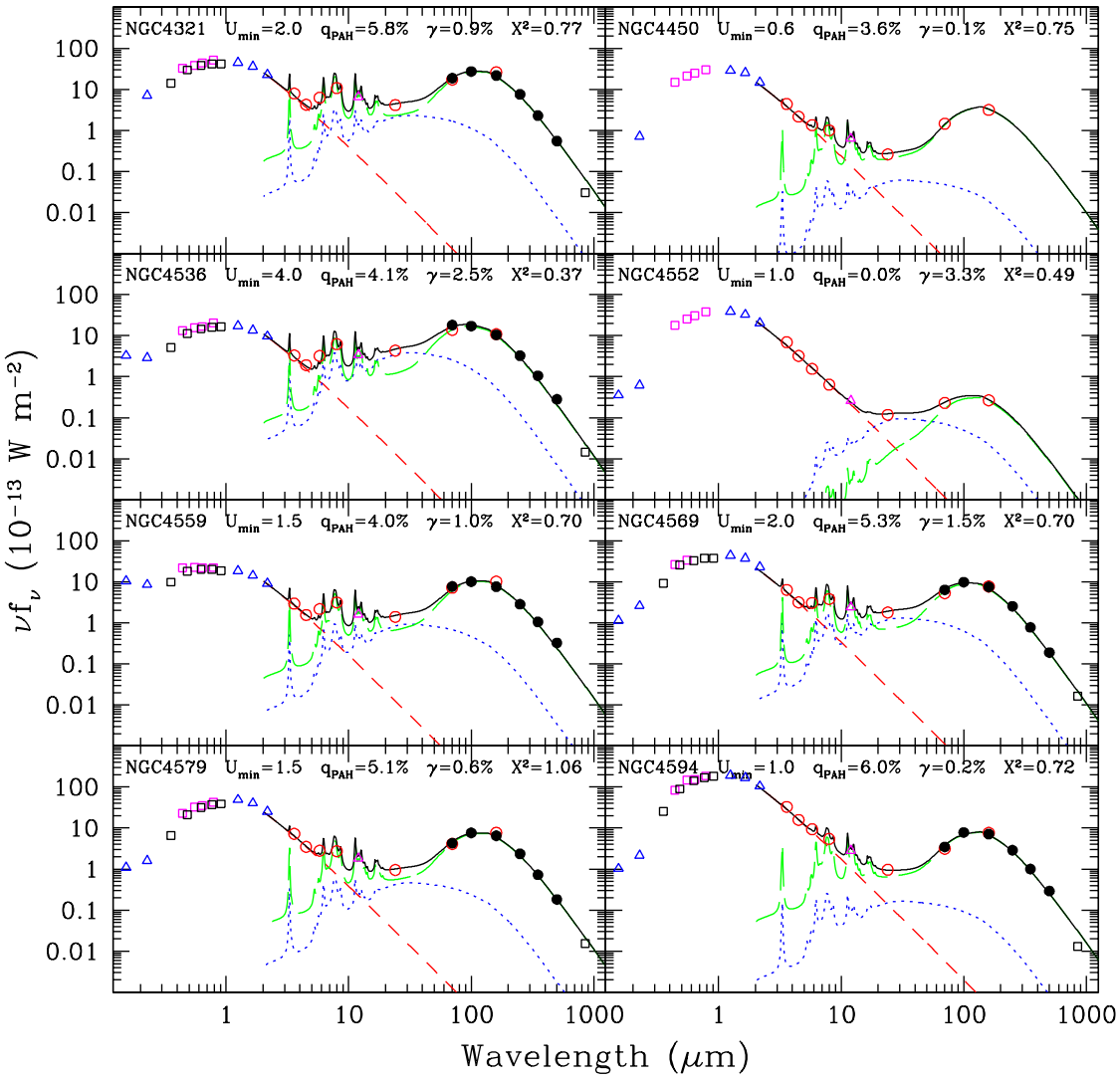

Figure 3. Globally-integrated infrared/sub-millimeter spectral energy distributions for the KINGFISH sample (continued).

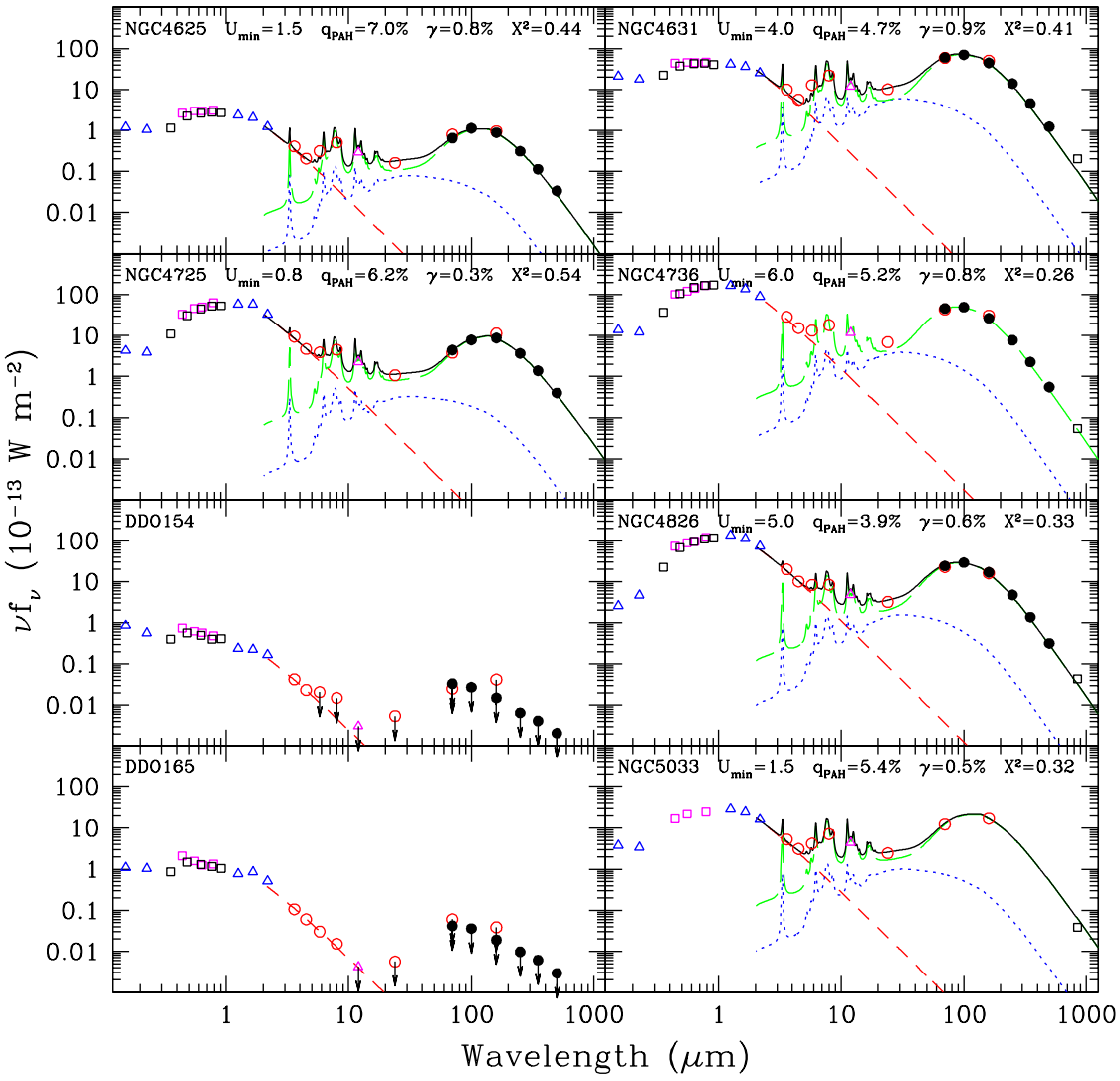

Figure 3. Globally-integrated infrared/sub-millimeter spectral energy distributions for the KINGFISH sample (continued).

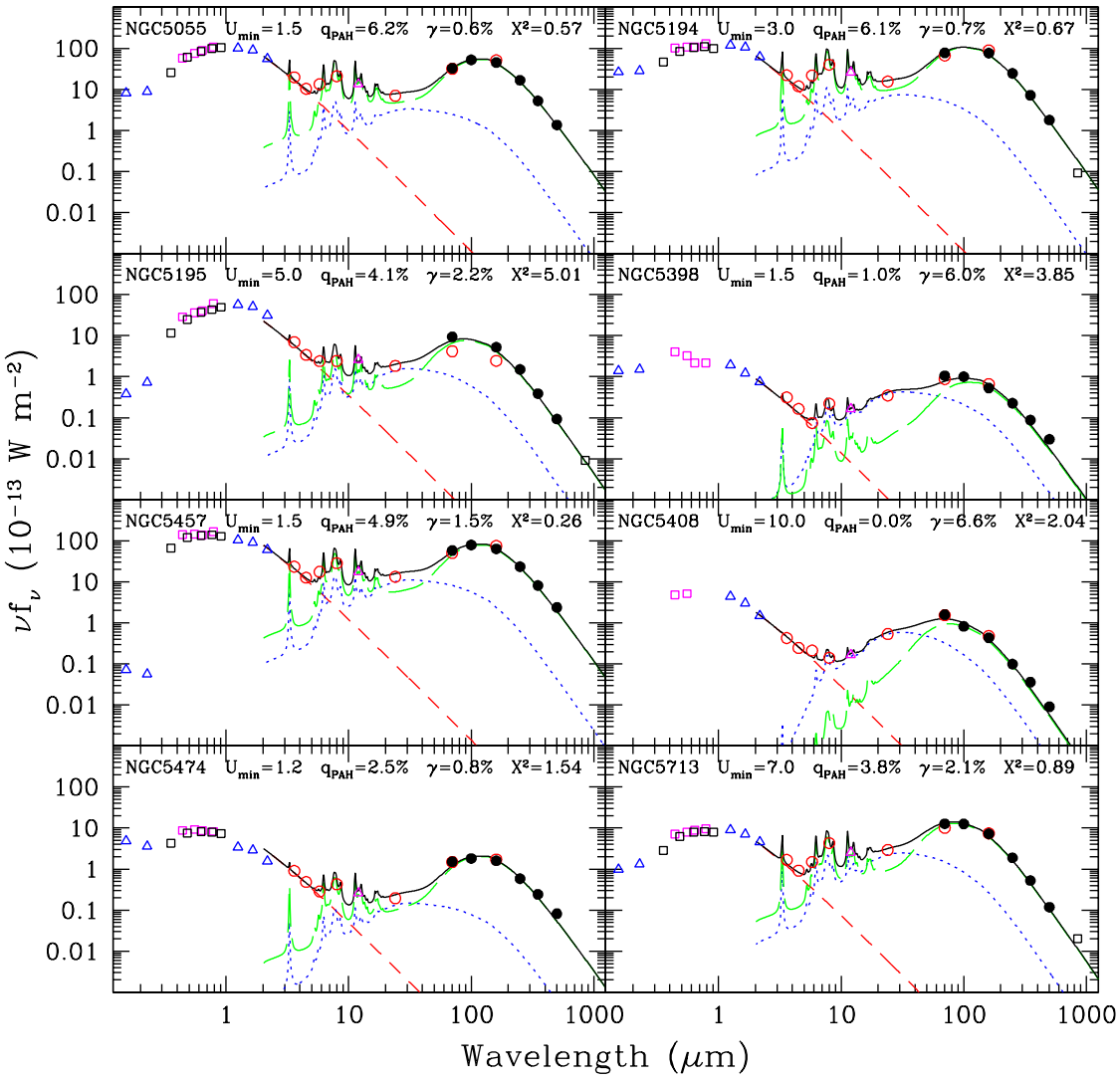

Figure 3. Globally-integrated infrared/sub-millimeter spectral energy distributions for the KINGFISH sample (continued).

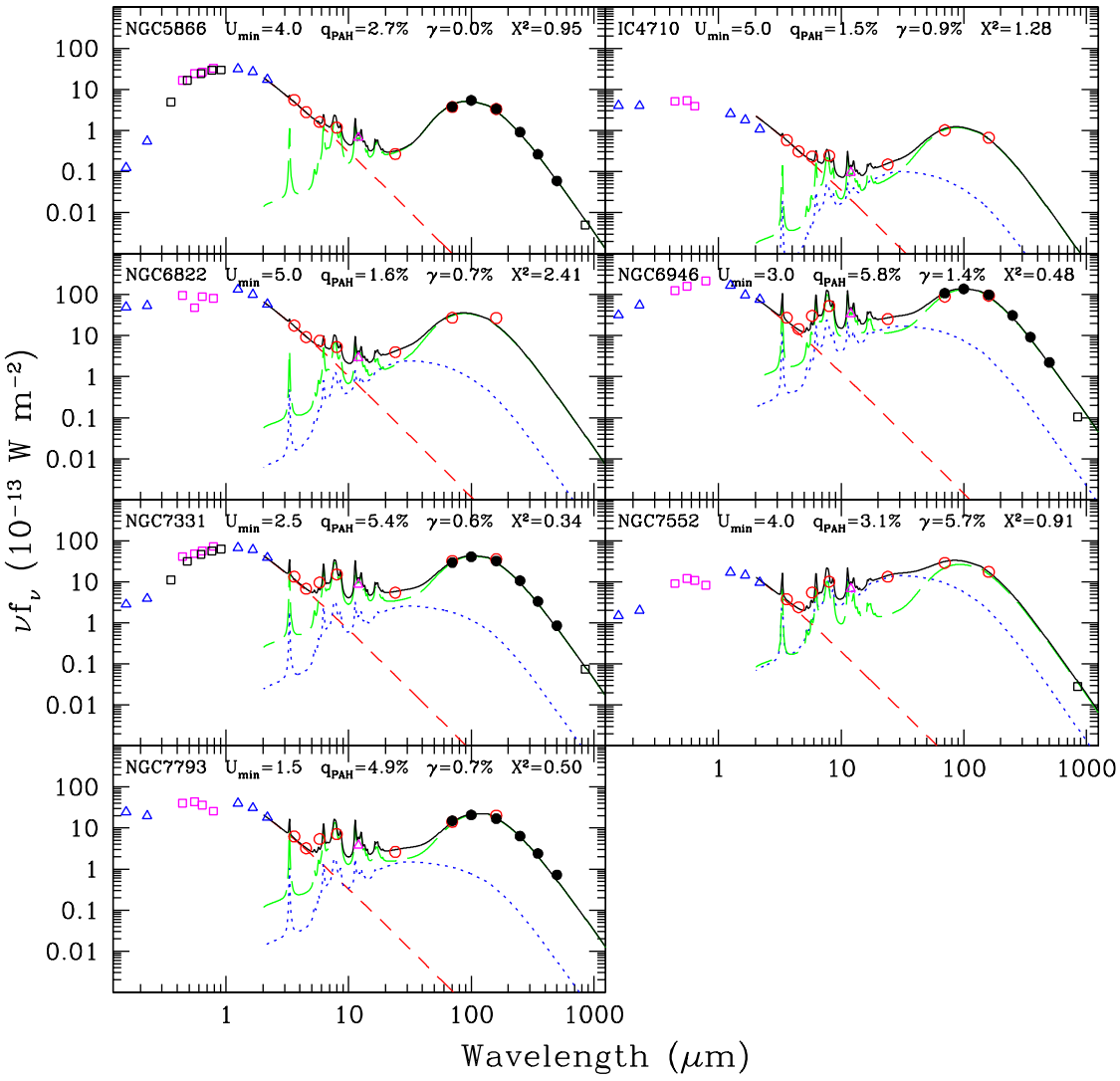

Figure 3. Globally-integrated infrared/sub-millimeter spectral energy distributions for the KINGFISH sample (continued).